High-dimensional imaging of the HPV-induced tumor microenvironment to improve clinical outcomes

Abdulrahman, Z.

PART II

SURVIVAL AND TME OF HPV-INDUCED CANCER PATIENTS

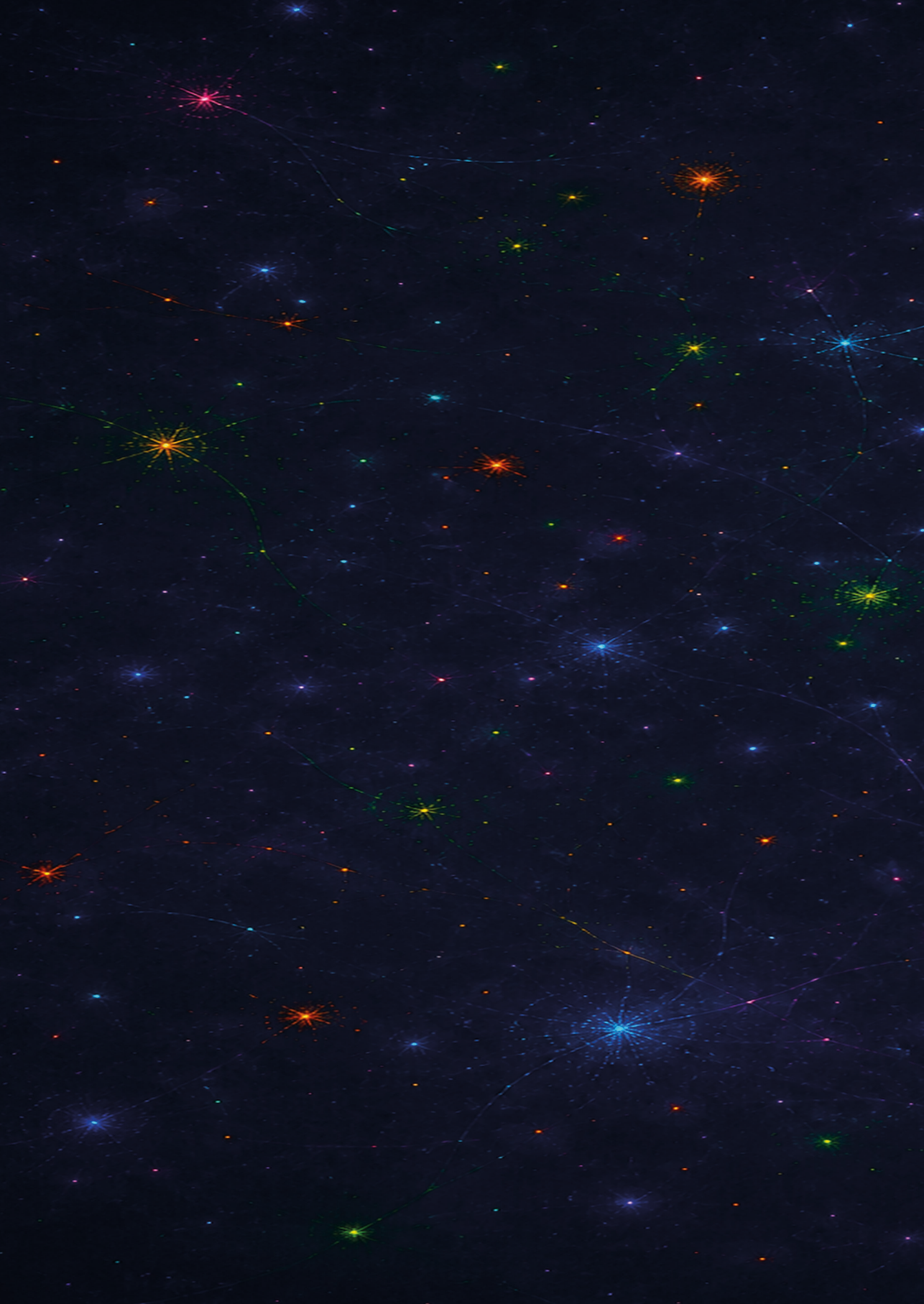

Chapter 7

Monocyte infiltration is an independent positive prognostic biomarker in vulvar squamous cell carcinoma

Ziena Abdulrahman, Kim E. Kortekaas, Marij J.P. Welters,
Mariette I.E. van Poelgeest, Sjoerd H. van der Burg

Cancer Immunology, Immunotherapy 2024

Key findings

- Vulvar squamous cell carcinoma (VSCC) is an aggressive disease, currently treated with limited success by mutilating therapies. Immunotherapy is studied as an alternative treatment option but its successful application requires in-depth knowledge of the spontaneous immune response in VSCC.
- Here, we identified for the first time that monocyte infiltration forms an independent positive prognostic marker for patient survival.
- Patients of whom their tumor is strongly infiltrated with both monocytes and T cells display the best survival and as such are likely to form excellent candidates for neoadjuvant immunotherapy.

Abstract

Background

Vulvar squamous cell carcinoma (VSCC) arises after an HPV infection or the mutation of p53 or other driver genes, and is treated by mutilating surgery and/or (chemo)radiation, with limited success and high morbidity. In-depth information on the immunological make up of VSCC is pivotal to assess whether immunotherapy may form an alternative treatment.

Methods

A total of 104 patient samples, comprising healthy vulva (n=27) and VSCC (n=77), were analyzed. Multispectral immunofluorescence (15 markers) was used to study both the myeloid and lymphoid immune cell composition and this was linked to differences in transcriptomics (NanoString nCounter, 1258 genes) and in survival (Kaplan Meier analyses).

Results

Healthy vulva and VSCC are both well infiltrated but with different subpopulations of lymphoid and myeloid cells. In contrast to the lymphoid cell infiltrate, the density and composition of the myeloid cell infiltrate strongly differed per VSCC molecular subtype. A relative strong infiltration with epithelial monocytes ($HLADR^{-}CD11c^{-}CD14^{+}CD68^{-}CD163^{-}CD33^{-}$) was prognostic for improved survival, independent of T cell infiltration, disease stage or molecular subtype. A strong infiltration with T cells and/or monocytes was associated with drastic superior survival: 5-year survival >90% when either one is high, versus 40% when both are low ($p<0.001$).

Conclusion

A hot myeloid and/or lymphoid infiltrate predicts excellent survival in VSCC. Based on the response of similarly high-infiltrated other tumor types, we have started to explore the potential of neoadjuvant checkpoint blockade in VSCC.

Introduction

Vulvar squamous cell carcinoma (VSCC) can arise due to three distinct etiological pathways, each with differential clinical prognosis: driven by classical oncogenic mutations in TP53 (HPV$^-$p53mut VSCC, poorest clinical outcome), driven by other somatic oncogenic mutations (HPV$^-$p53wt, intermediate clinical outcome), or driven by a persistent infection with the oncogenic human papillomavirus (HPV$^+$ VSCC, best clinical outcome).[1 2] The current standard of care for VSCC is surgery and/or (chemo)radiation, which is associated with high morbidity due to severe local or systemic side effects. Therefore, novel treatment strategies are urgently needed.

Immunotherapy is increasingly being explored as an alternative for current standard cancer treatments. Studies in other tumor types have shown the importance of a pre-existing well-coordinated immune response for the prognosis and response to immunotherapy of cancer patients.[3 4] Also in vulvar high-grade squamous intraepithelial lesions (vHSIL), the precursor lesion of HPV$^+$ VSCC, the prerequisite of a pre-existing well-coordinated hot immune microenvironment for response to different forms of immunotherapy has been identified.[1 5 6]

In VSCC, the presence and impact of lymphoid cells on prognosis has been studied before[7] and revealed that the presence of high numbers of CD3$^+$CD8$^-$ FOXP3$^-$ T helper cells is an independent prognostic marker for survival, regardless of molecular subtype. Furthermore, higher T cell infiltration was associated with the expression of higher myeloid cell associated transcripts.[8] So far only two studies have analyzed myeloid cells in VSCC, reporting the association between high numbers of CD68$^+$ macrophages and low grade VSCC, and the presence of low CD1a$^+$ dendritic cell numbers with recurrent VSCC.[9 10] However, these studies were based on single marker immunohistochemistry in small patient cohorts, hence no in-depth insight in the actual myeloid cell composition of VSCC is available.

Here we aimed to fill that gap by an in-depth investigation of the myeloid and lymphoid infiltration in VSCC, using multispectral immunofluorescence and transcriptome analysis. Our study on a large sample set of healthy vulvar tissue and VSCC revealed that the type and number of VSCC infiltrating myeloid cells is linked to the molecular subtype of VSCC. High epithelial infiltration

by $CD14^+CD68^-CD11c^-$ monocytes formed a strong prognostic biomarker for excellent survival of VSCC patients, independent from $CD3^+$ T cell infiltration.

Materials and methods

Patient samples

Formalin-fixed paraffin-embedded (FFPE) tissue of n=104 women of ≥18 years old with histologically confirmed healthy HPV-negative vulva (n=27) or VSCC (n=77) were included. The healthy HPV^- vulvar tissue was from anonymized women who underwent labiaplasty. The included VSCC patients had FIGO stage I-IIIB at diagnosis, were treated with standard of care (surgical excision, and if needed adjuvant radiotherapy) at a tertiary hospital in the Netherlands, and all patients underwent 5 years of follow-up. All the tumor material investigated in this study was obtained prior to therapy. The study was in accordance with the Declaration of Helsinki, and approved by the local medical ethical committee of the Leiden University Medical Center (LUMC) and in agreement with Dutch law. HPV, P16 and P53 typing on all formalin-fixed paraffin-embedded (FFPE) tumor sections was performed as described before.[7] HPV^+p53mutant VSCC were not observed in our cohort. Routine diagnostic beta-catenin immunohistochemical staining was performed on 10 VSCC patients. A summary of the patient characteristics, treatments and performed tumor analyses is provided in **Supplemental Table 1 and 2**.

Multispectral immunofluorescence staining

A previously developed seven-color multispectral immunofluorescence panel for myeloid cells was applied, consisting of CD14, CD33, CD68, CD11c, CD163, HLA-DR, DAPI.[6] In this panel a combination of direct detection (primary antibody directly labelled with fluorochrome) and indirect detection (fluorochrome labelled secondary antibody) of markers was used for fluorescence microscopy. An overview of the antibodies and staining methods included in each panel are shown in **Supplemental Table 3**. Briefly, 4µm FFPE tissue sections were deparaffinized, endogenous peroxidase was blocked with hydrogen peroxide and heat induced epitope retrieval was performed with tris-EDTA (10mM/1mM, pH 9.0). SuperBlock (ThermoFisher Scientific) was used to block non-specific binding sites. First, the antibodies detected by Opal were applied, followed by the unconjugated antibodies which were incubated overnight. On the second day the corresponding fluorescently labelled secondary antibodies were applied, followed by 5 hours incubation with the directly labeled primary

antibodies. Finally, DAPI was applied as nuclear counterstain and slides were mounted.[6]

Quantification of immune cells in the TME

As published[5], images of the entire tissue sections stained with the multispectral immunofluorescence panels were acquired with the Vectra 3.0.5 multispectral imaging microscope (PerkinElmer) at 20x magnification. Immune cells in the TME were automatically phenotyped and counted with inForm 2.4 image analysis software (PerkinElmer-Akoya Biosciences) after manual training. The software was trained to segment epithelium and stroma, segment $DAPI^+$ nucleated cells, and assign a phenotype to each cell. All phenotypes were visually inspected on accurateness, and if errors were detected the training was further optimized until all discrepancies were resolved. Immune cell counts were normalized for tissue size (cells/mm^2 epithelium and cells/mm^2 stroma). A threshold of a median cell count ≥10 cells/mm^2 in at least one tissue category was applied to study biologically common phenotypes.

Transcriptomic analyses

The archived diagnostic FFPE tissue blocks were used to cut sections of 10µm for RNA extraction.[8] Directly before and after these 10µm thick sections, a 4µm section was cut for hematoxylin-eosin (HE) staining. A pathologist annotated the tumor regions on the HE slides to ensure that the slides contained tumor. After the sections were deparaffinized, the tumor areas were macro-dissected using the annotated HE slides as reference. RNA was then isolated with the RNA FFPE isolation kit (Qiagen), according to the manufacturer's instructions. The quality and quantity of the RNA was verified with the Agilent 2100 Bioanalyzer System, using the RNA 6000 Nano kit (Agilent). Samples were selected for further processing when >20% of the RNA fragments were >300bp and the corrected RNA concentration remained ≥60µg/µl.

To measure the gene expression profiles, 300ng of RNA from each sample was hybridized with the probes of the human PanCancer panel (730 genes) or IO360 panel (750 genes) for 17 hours at 65°C, following the manufacturer's instructions (NanoString). The number of copies of each gene in every sample was counted by scanning 490 Fields Of View using the NanoString nCounter MAX system. The raw data (counts of genes) were uploaded to the Rosalind platform, after which quality checks were performed. The housekeeping genes in the panels facilitated sample-to-sample normalization. Eight negative controls and six synthetic positive controls were included. The data were

reviewed for reliability and validity based on the imaging (>0.75) and binding density (0.1-2.25) quality control metrics, and performance check of the positive controls (0.95-1). Benjamini-Hochberg adjusted p-values were used to decrease the false-discovery rate. Differentially expressed genes (DEGs) were defined by a log2 fold difference of >1 or ≤1 and a p-value<0.05.

Gene ontology analysis of the differentially expressed genes (DEGs) was performed with ClueGo.[11]

Gene Set Enrichment Analysis (GSEA) was performed with the Broad Institute GSEA software package and collections for human gene sets, version 4.3.2.[12 13] 1000 permutations were applied, and small gene sets were excluded by applying a threshold of at least 15 genes. Gene sets with an FDR<0.25 as well as p-value<0.05 were selected.

Statistical analyses

Statistical data analysis was performed with GraphPad Prism 9.3.1, which was also used to create graphs to visualize the data. The median immune counts of three different VSCC molecular subtypes were compared with the non-parametric Kruskal Wallis test, of two subgroups with the non-parametric Mann-Whitney U test. Spearman correlation was used to study correlations between the T cell and myeloid cell infiltrate. Kaplan Meier survival analyses were performed with SPSS 25.0. Differences in survival and hazard ratio (HR) with 95% confidence interval, were calculated with the non-parametric Mantel-Cox test. Two-sided p-values<0.05 were marked as statistically significant.

Results

A diverse myeloid cell infiltration is present in VSCC

An earlier transcriptomic study suggested that stronger T cell infiltration in VSCC was associated with more myeloid cell infiltration[8], but the actual composition and location of the myeloid cell infiltrate was unknown. Therefore, a multispectral myeloid cell immunofluorescence panel, recently shown to be helpful in understanding the clinical response of vHSIL patients to different forms of immunotherapy[5 6], was applied to a large set of 77 VSCC patients **(Figure 1A)**.

Based on the markers CD68, CD163, HLADR, CD11c, CD14 and CD33 used, at least 16 different phenotypes of myeloid cells that infiltrated VSCC were identified. To simplify their notation, the positively stained markers are indicated with a '+', whereas markers that were negative are indicated as 'rest-'. The presence of $CD14^{+}rest^{-}$ monocytes, $CD68^{+}rest^{-}$ macrophages, and $HLADR^{+}CD11c^{+}rest^{-}$ dendritic cells was most prominent in the epithelium. The stroma of VSCC contained most of the phenotypes and was richly infiltrated by the three afore mentioned myeloid cell subtypes. In addition, $CD68^{+}rest^{-}$ macrophages and $CD68^{+}CD163^{+}rest^{-}$ M2-like macrophages were detected **(Figure 1B)**. However, there was a large diversity regarding the numbers of tumor-infiltrating myeloid cells across the 77 patients.

Subgroup analysis based on early stage (FIGO I/II) versus late stage (FIGO III) VSCC showed no differences in epithelial myeloid cell infiltration. However, in the stromal compartment of late stage VSCC, a significant decrease in $CD14^{+}CD33^{-}rest^{-}$ monocytes, $HLADR^{+}rest^{-}$ cells, $HLADR^{+}$ $CD14^{+}rest^{-}$ monocytes, $HLADR^{+}CD11c^{+}rest^{-}$ dendritic cells, $HLADR^{+}CD11c^{+}CD14^{+}rest^{-}$ dendritic cells (DCs), $CD68^{+}$ $CD14^{+}rest^{-}$ inflammatory macrophages, $CD68^{+}$ $HLADR^{+}CD11c^{+}rest^{-}$ cells, $CD68^{+}$ $HLADR^{+}CD11c^{+}CD14^{+}rest^{-}$ M1-like macrophages, $CD68^{+}CD163^{+}HLADR^{+/-}$ $^{-}CD14^{+}rest^{-}$ M2-like macrophages, and $CD68^{+}CD163^{+}HLADR^{+}CD11c^{+}CD14^{+}CD33^{-}$ M2-like macrophages was observed **(Figure 1C)**. This indicates that during progression of VSCC from early to late stage, the tumor may become colder in terms of myeloid cell infiltration **(Supplemental Table 4)**.

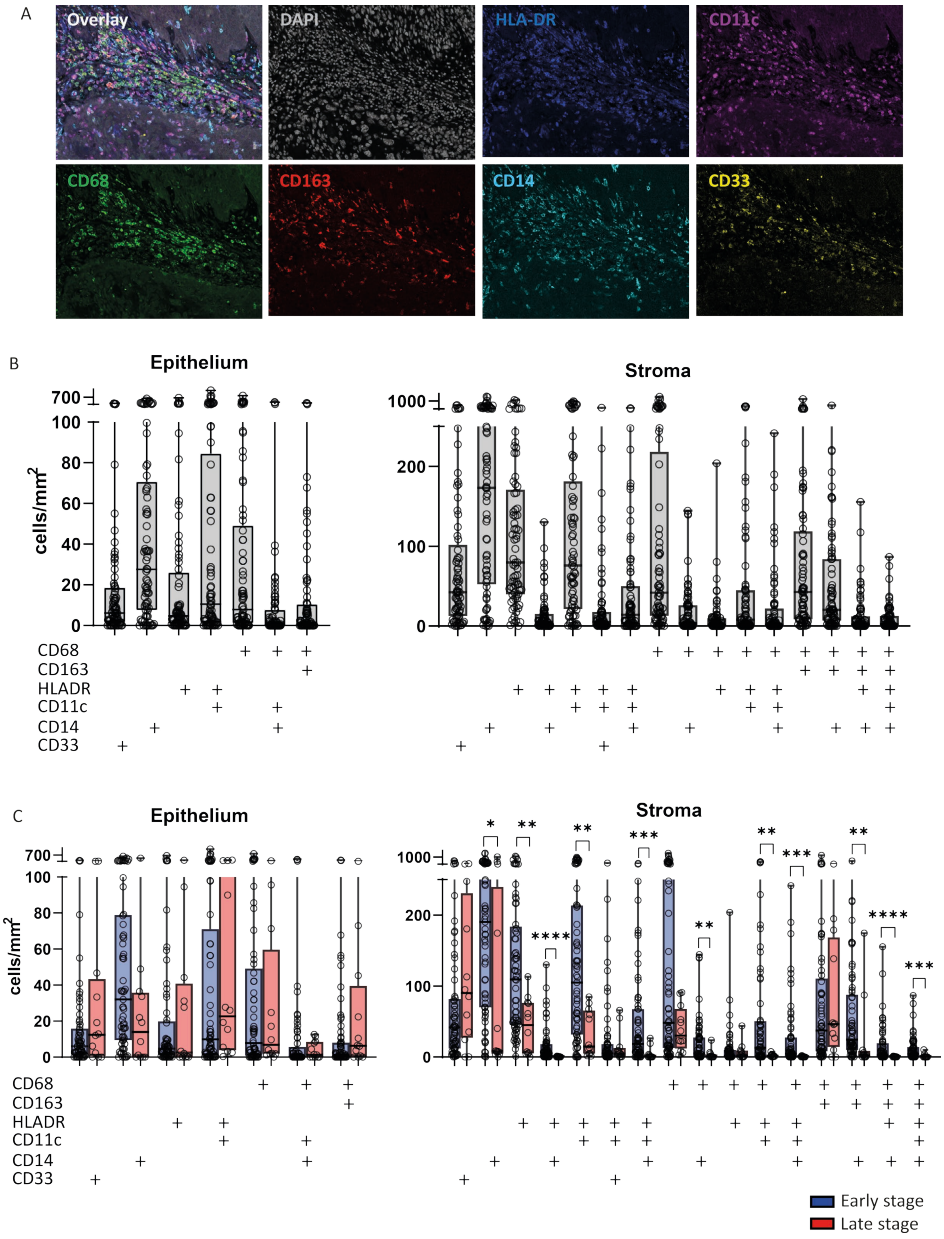

Figure 1. Identification and quantification of myeloid cells in VSCC.

***A**) Multispectral immunofluorescence staining of myeloid cells in VSCC, single markers staining and overlay. **B**) Myeloid cell phenotypes and quantification in the total VSCC cohort (n=77). **C**) Myeloid cell phenotypes and quantification in early (FIGO I/II in blue, n=65) versus late (FIGO III in red, n=12) stage VSCC. Boxplots with middle line indicating median, colored box indicating interquartile range, vertical lines from minimum to maximum cell count value. Marker+ indicates its expression by that specific cell phenotype. Asterisks indicate statistically significant differences (* p<0.05,** p<0.01, *** p<0.001, **** p<0.0001).*

Molecular subtype specific myeloid cell attraction in vulvar cancer

VSCC can be subdivided into three different molecular subtypes which are correlated to survival, based on the presence of HPV and the TP53 status: HPV$^-$p53mutant, HPV$^-$p53wildtype and HPV$^+$. To assess if the increased myeloid cell infiltrate in VSCC was a general phenomenon or specific for a molecular subtype, the myeloid cell numbers and composition in each subgroup were studied. HPV$^+$ VSCC had a higher number of total infiltrating myeloid cells (both intraepithelial and stromal), with especially more CD14$^+$rest$^-$ monocytes, HLADR$^+$CD11c$^+$CD14$^+$rest$^-$ inflammatory DCs and CD68$^+$ rest$^-$ macrophages, but less CD68$^+$CD163$^+$rest$^-$ M2-like macrophages when compared to the HPV$^-$ subtypes. HPV$^-$p53wt VSCC had more stromal HLADR$^+$ CD14$^{+/-}$rest$^-$ cells, HLADR$^+$CD11c$^+$CD14$^{+/-}$CD33$^+$ dendritic cells, CD68$^+$ HLADR$^{+/-}$ CD14$^{+/-}$rest$^-$ M1-like macrophages and CD68$^+$CD163$^+$HLADR$^{+/-}$ CD14$^{+/-}$rest$^-$ M2-like macrophages compared to HPV$^-$p53mut VSCC **(Figure 2AB, Supplemental Table 5A, Supplemental Figure 1)**. Twenty out of 23 myeloid subpopulations were statistically significantly different between the VSCC molecular subtypes. In contrast, re-analysis of the number and composition of detected subpopulations of infiltrating T cells[7] showed that they did not grossly differ across the molecular subtypes of VSCC **(Figure 2C, Supplemental Table 5B, Supplemental Figure 2, Supplemental Figure 3A)**.

Since coordination of immunity has been a well-established prognosticator for survival and response to immunotherapy[3 6 14], we analyzed the correlations between the lymphoid and myeloid cell infiltrate. No clear correlations were found between lymphoid and myeloid cell infiltration in all VSCC molecular subtypes, except for a weak but significant correlation between stromal CD3$^+$PD1$^+$ T cells and epithelial CD14$^+$rest$^-$ myeloid cells in HPV$^+$ VSCC **(Supplemental Figure 4)**.

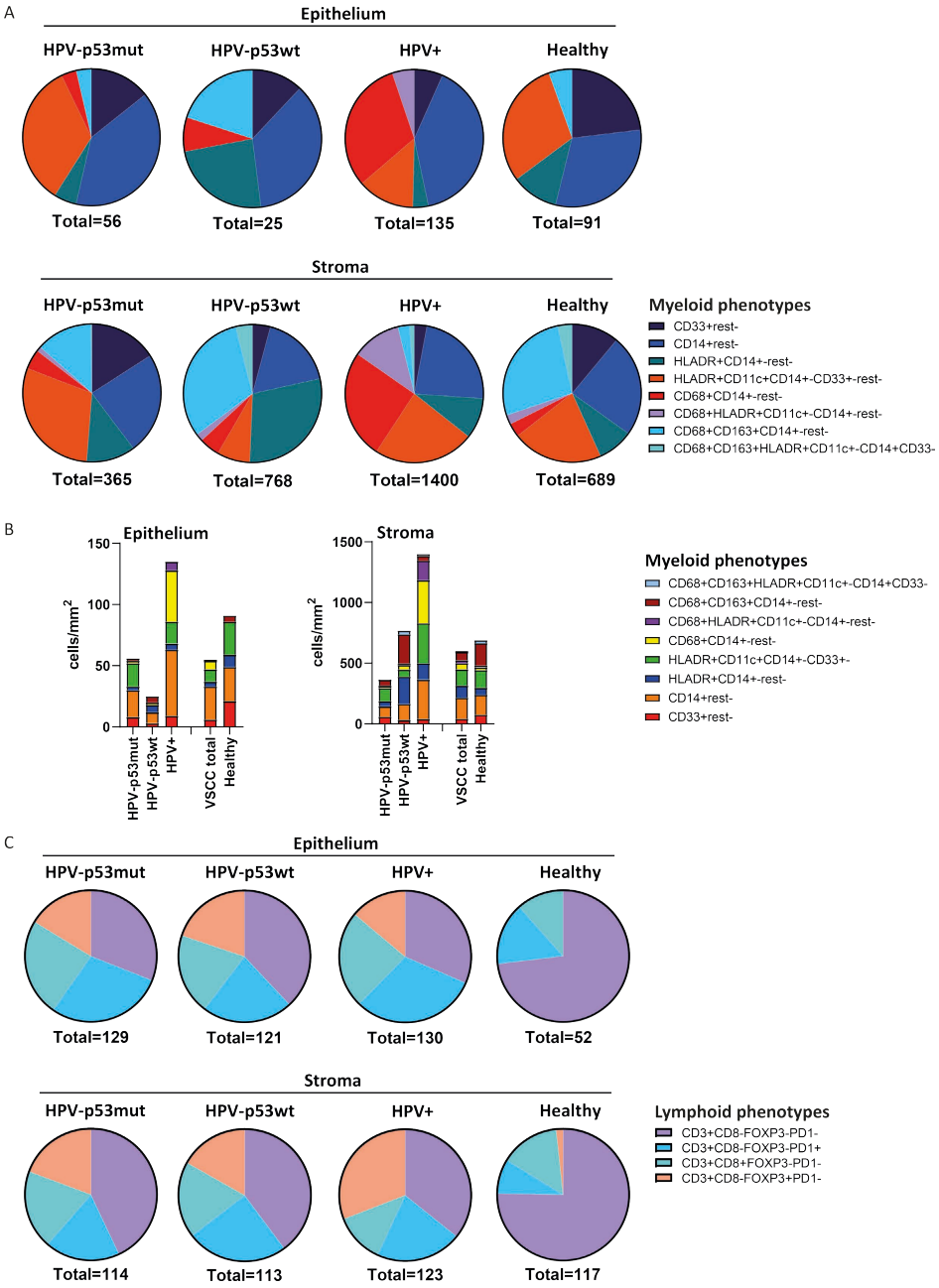

Figure 2. Myeloid and lymphoid immune composition differences per VSCC molecular subtype.

*The myeloid cell composition **A**) fractionally and **B**) quantitatively, as well as **C**) the lymphoid cell composition fractionally in the epithelium and stroma of HPV$^-$p53mut VSCC (n=31), HPV$^-$p53wt VSCC (n=21), HPV$^+$ VSCC (n=25) and healthy HPV$^-$ vulva (n=10). Number below the graphs indicates the median total number of cells/mm^2. Cell types are indicated by the markers (CD68, CD163, HLADR, CD11c, CD14, CD33) staining positive, markers not stained are indicated as 'Rest-'.*

Key myeloid cell phenotypes impacting survival in VSCC

We performed Kaplan Meier survival analyses using the median counts of each myeloid cell phenotype to split the total VSCC cohort into high or low infiltrated. This revealed 3 myeloid cell phenotypes that strongly correlated with survival **(Figure 3A, Supplemental Figure 5)**. The strongest separation of the survival curves was observed for epithelial CD14$^+$rest$^-$ monocytes and stromal CD14$^+$CD11c$^+$HLADR$^+$rest$^-$ inflammatory DCs (both p-value = 0.001) **(Figure 3A)**. Patients from all three molecular subtypes were represented in these myeloid cell high and low groups **(Figure 3B)**. Intriguingly, patients with VSCC in which the function of p53 (in)directly is impaired (HPV$^+$ or HPV$^-$p53mut) more often showed high infiltration with epithelial CD14$^+$rest$^-$ monocytes and stromal CD14$^+$CD11c$^+$HLADR$^+$rest$^-$rest$^-$ inflammatory DCs, compared to HPV$^-$ p53wt VSCC **(Figure 3B)**. Functional loss of p53 in cancer cells has previously been linked to enhanced recruitment of myeloid cells to the tumor site.[15-17]

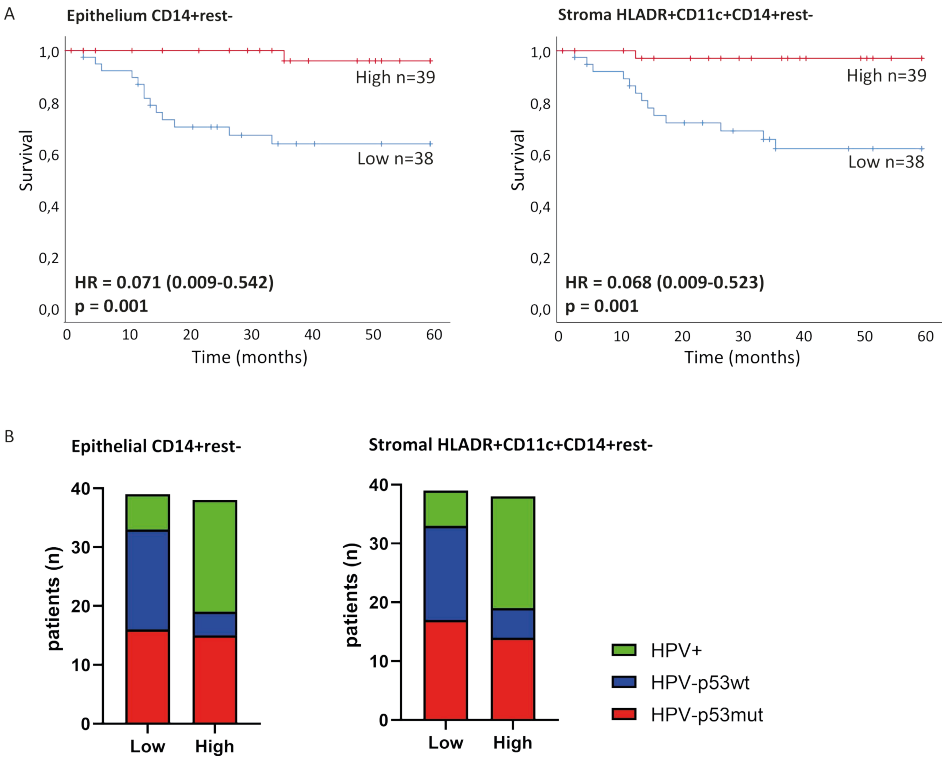

Figure 3. Pro-inflammatory myeloid cell composition predicts excellent survival in VSCC.

***A**) Kaplan Meier survival curves for VSCC (n=77) with high or low myeloid cell infiltration, including hazard ratio (HR, between brackets the 95% confidence interval of the hazard ratio is provided), and p-value. Total VSCC cohort split by median into high versus low counts. Left survival curve for separation by CD14⁺rest⁻ monocyte infiltration, low infiltration (blue): HPV⁻p53mut n=16, HPV⁻p53wt n=17, HPV⁺ n=6, high infiltration (red): HPV⁻p53mut n=15, HPV⁻p53wt n=4, HPV⁺ n=19. Right survival curve for separation by stromal HLADR⁺CD11c⁺CD14⁺rest⁻ dendritic cell infiltration, low infiltration (blue): HPV⁻p53mut n=17, HPV⁻p53wt n=16, HPV⁺ n=6, high infiltration (red): HPV⁻p53mut n=14, HPV⁻p53wt n=5, HPV⁺ n=19. **B**) Distribution of VSCC molecular subtypes (n=77 total) across low versus high (split by median) epithelial CD14⁺rest⁻ monocyte infiltration (left graph), and stromal HLADR⁺CD11c⁺CD14⁺rest⁻ dendritic cell infiltration (right graph).*

Transcriptomic differences in myeloid hot versus cold tumors

In order to gain more insight into what may underly the difference between specific myeloid cell phenotype hot and cold tumors, we combined the transcriptomic data (1258 different individual genes) of a group of 44 VSCC patients, containing both early and late stage patients, and all three molecular subtypes[8]. These patients were divided in two groups based on the median epithelial CD14⁺rest⁻ monocyte cell count or the stromal CD14⁺CD11c⁺HLADR⁺rest⁻ inflammatory DC count, and the differentially expressed genes (DEGs) between the myeloid hot versus cold groups were

analyzed. This rendered a total of 97 DEGs between the epithelial CD14^{+}rest^{-} monocyte high versus low group **(Figure 4A, Supplemental Table 6)**, and a total of 62 DEGs between the stromal inflammatory DC high versus low group **(Figure 4A, Supplemental Table 7)**, using a threshold of fold change difference >1.5 and p-value <0.05. 29 DEGs were present in both comparisons. The great majority of DEGs were higher expressed in myeloid cold tumors (75 and 37, respectively).

In contrast to the stromal region, the epithelial region is unambiguously demarcated and as such, more reproducible to define across studies. Therefore, we focused on the epithelial CD14^{+}rest^{-} monocytes high/low separation in subsequent analyses. The DEGs between CD14^{+}rest^{-} monocyte high and low VSCCs comprised a number of cytokines, including increased expression of *CXCL8* and *CCL20,* known to attract monocytes[18 19], as well as the inducers of inflammation *IL-1α* and *IL-1β* **(Supplemental Table 6)***,* previously reported to be upregulated in tumors that have lost p53 function[15]. The cytokines *IL-34, CCL14* and *CCL19* that were overexpressed in the CD14^{+}rest^{-} monocyte low VSCC **(Supplemental Table 6)** are not known to recruit monocytes. Analysis of the differentially expressed cytokines revealed no overt differences between the VSCC molecular subtypes **(Supplemental Figure 6)**.

To analyze which underlying signaling pathways were activated in these myeloid hot and cold tumors, ClueGo gene ontology analysis and Hallmark Gene Set Enrichment Analysis (GSEA) was performed. The majority of upregulated genes in CD14^{+}rest^{-} monocyte cold tumors were involved in organogenesis pathways, including 'pluripotent stem cell differentiation pathway', 'embryonic stem cell pluripotency pathway', 'WNT signaling pathway and pluripotency'. In CD14^{+}rest^{-} monocyte hot tumors the majority of upregulated genes were involved in pro-inflammatory pathways **(Figure 4B, Supplemental Figure 7)**. The GSEA revealed that epithelial monocyte hot VSCCs displayed a gene set upregulated in the response to UV, known to lead to monocyte attraction[20]. In contrast, epithelial monocyte cold VSCCs were characterized by the upregulation of genes involved in adipogenesis and in the oncogenic KRAS, WNT and TGFβ signaling pathways **(Figure 4C)**. However, the upregulation of the WNT pathway in monocyte cold VSCC could not be confirmed at the protein level by beta-catenin immunohistochemistry **(Supplemental Figure 8)**.

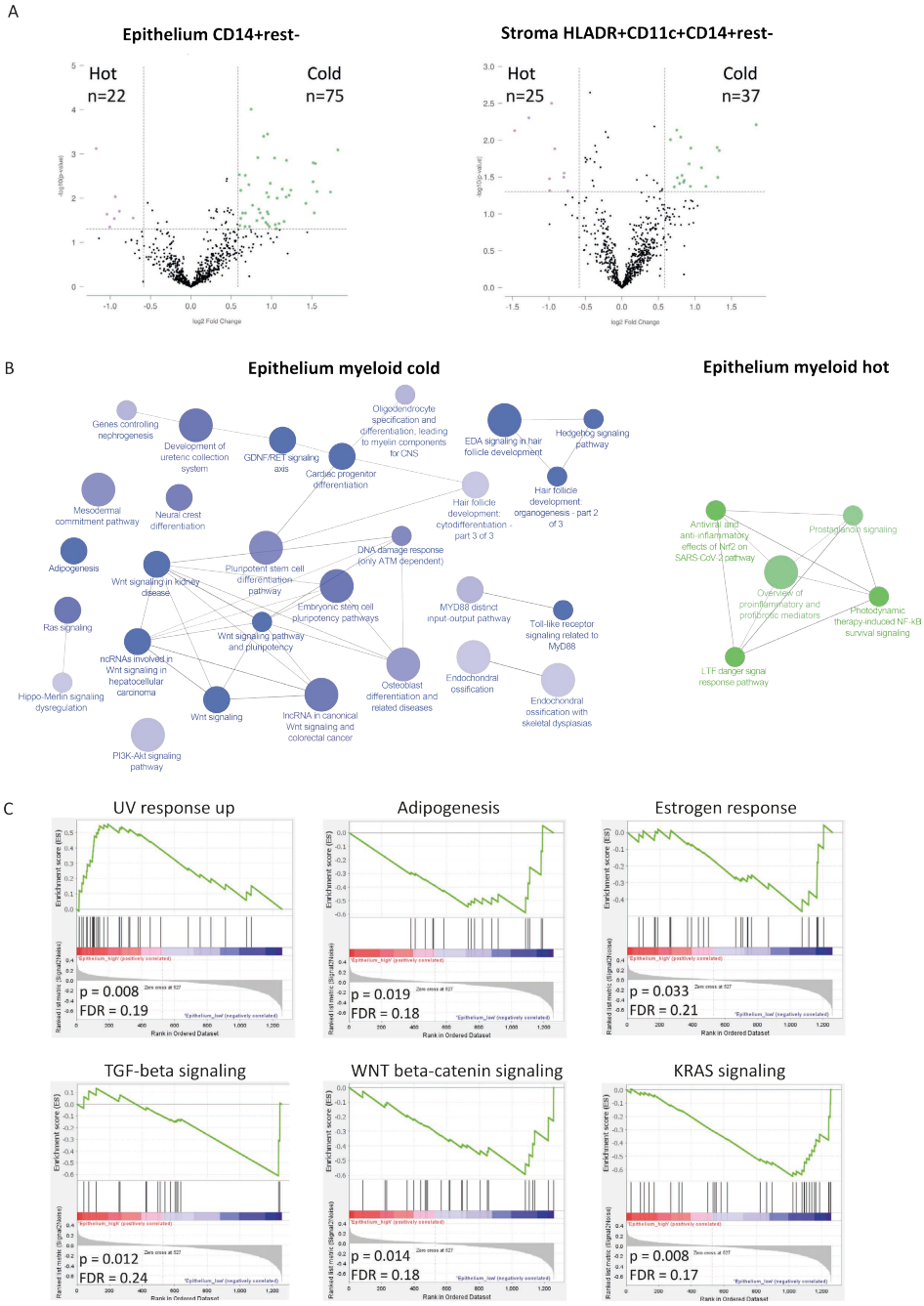

Figure 4. Transcriptomic differences between myeloid hot and cold tumors.

***A**) Volcano plots of differentially expressed genes (DEGs) between myeloid hot versus cold VSCC lesions (total VSCC n=77, split by median into hot or cold): epithelial CD14⁺rest⁻ monocytes (left graph) and stromal HLADR⁺CD11c⁺CD14⁺rest⁻ dendritic cells (right graph). **B**) ClueGo pathway analysis of identified*

*DEGs between epithelial CD14^{+}rest^{-} monocytes hot versus cold VSCC. **C**) Hallmark gene set enrichment analysis (GSEA), showing gene sets enriched in epithelial CD14^{+}rest^{-} hot versus cold VSCC, selected based on FDR<0.25 as well as p<0.05.*

Myeloid and T cell counts are independent predictors for excellent survival in VSCC

Previously it was described that HPV^{-}p53mut VSCC patients have the poorest survival, HPV^{-}p53wt VSCC patients an intermediate survival, and HPV^{+} VSCC patients an excellent survival[2], similar to our study cohort **(Supplemental Figure 9)**. In addition, epithelial CD3^{+} T cell infiltration was reported to be prognostic in VSCC, irrespective of tumor stage and molecular subtype.[7 8] As there was no direct correlation between epithelial T cell infiltrate and either identified myeloid cell subpopulation **(Figure 5A)**, we explored whether the combination of intraepithelial T cell infiltration with both myeloid cell subpopulations would provide more insight into the prognostic role of either.

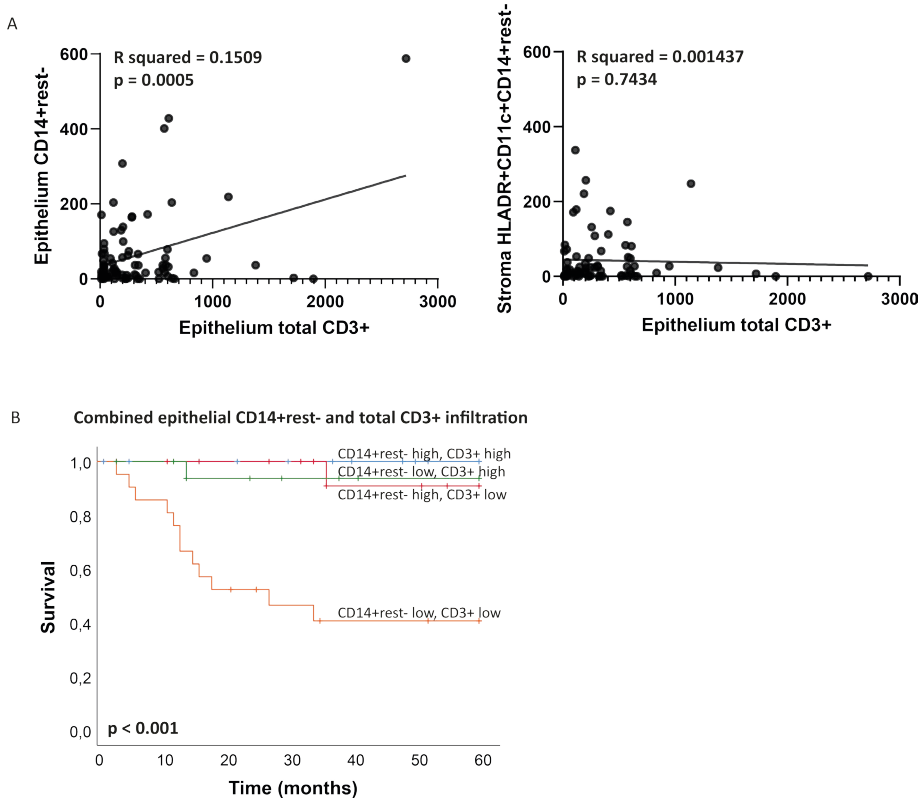

Figure 5. High myeloid cell and T cell infiltration are independent predictors for excellent survival.

***A**) Pearson correlation plots between myeloid (epithelial CD14$^+$rest$^-$ or stromal HLADR$^+$CD11c$^+$CD14$^+$rest$^-$) and lymphoid cell infiltrate (epithelial total CD3$^+$) in VSCC (n=77). **B**) Kaplan Meier survival curves for VSCC patients with differential lymphoid (epithelial total CD3$^+$) and myeloid (epithelial CD14$^+$rest$^-$) cell infiltration (total VSCC n=77, split by respective medians into hot or cold).*

Multivariate analyses with tumor stage, molecular subtype, intraepithelial T cell infiltration and either one of the myeloid populations (epithelial monocytes and stromal inflammatory DCs) showed that both myeloid cell types could function as prognostic factors **(Table 1)**. However, analysis of all three immune markers simultaneously revealed that both intraepithelial CD3$^+$ T cells and the intraepithelial CD14$^+$rest$^-$ monocytes were the only independent prognostic markers, irrespective of tumor stage and molecular subtype **(Table 1)**. An interaction analysis of both latter phenotypes, by splitting the patient group into four based on the median epithelium infiltrating CD3$^+$ T cell count (high/low[101]) and the median epithelium infiltrating CD14$^+$rest$^-$ monocyte count, revealed that the group of patients with a combined high CD3$^+$ T cell and high CD14$^+$rest$^-$ monocyte infiltration displayed the best survival, similar to the patient groups with a high infiltration of either one of these two immune cell types. The patient group with a low infiltration of both immune cell types displayed poorest survival **(Figure 5B)**. This revealed that the presence of a high epithelial CD14$^+$rest$^-$ monocyte infiltrate is equally important to that of T cells.

Discussion

The data from this first in-depth study of myeloid cell infiltration in a large group of VSCCs revealed that the composition of the myeloid cell infiltrate strongly differed per molecular subtype of VSCC, while this is not the case for lymphoid cell infiltrate[7]. Among the sixteen different identified phenotypes, two myeloid cell phenotypes were strongly associated with improved survival: epithelial monocytes and stromal dendritic cells. These myeloid cell subsets were found in higher numbers more often in VSCCs with loss of p53 function, either through interaction with the HPV oncoprotein E6 or via direct TP53 mutation. In comparison to all other known prognostic parameters (tumor stage, molecular subtype, intraepithelial T cell infiltration) only intraepithelial monocytes and T cells were independent prognostic factors in a multivariate analysis. A strong epithelial infiltration with either T cells or monocytes was associated with drastically improved clinical benefit, while low infiltration with both immune cell types was associated with poor survival.

It is well established that molecular features of the tumor may impact the immune composition of the TME.[15 21-26] While our earlier studies in VSCC revealed no overt impact of the different molecular subtypes on the number and composition of lymphocyte infiltration[7 9], our current study suggests that this is different for myeloid cells. There were clear differences with respect to the numbers and phenotypes of infiltrating myeloid cells between molecular subtypes. In particular patients with VSCC not caused by HPV or a TP53 mutation, were less likely to show strong infiltration with intraepithelial monocytes and stromal DCs, immune cell types both shown to be strongly associated with patient survival. Earlier studies have shown that loss of p53 function specifically resulted in the production of cytokines and attraction of innate leukocytes, the specific cytokine and innate cell types depending on the mouse models used[17 24], and included monocytes[16]. Our data suggest that in VSCC, functional loss of p53 may lead to the enhanced attraction of intraepithelial monocytes and stromal DCs.

At first sight it is surprising to find that the epithelial infiltration of VSCC with monocytes forms such a strong independent prognostic factor. However, monocytes attracted by CCL20 were shown to be essential for efficient cross-priming of T cells after mucosal or skin immunization, and preceded the sequential accumulation of $CD11c^+$ MHC class II^+ DCs in dermis and epithelium[19]. While there is evidence that monocytes may present the antigen directly to T cells[19], others have found that they were highly effective in transferring antigens to DCs in lymphoid tissue[27], in line with current concepts of antigen cross-priming[28]. Also in VSCC the increased presence of monocytes is associated with increased expression of CCL20 in tumors, making it a highly likely scenario that in VSCC monocytes may have a similar role. Interestingly, in esophageal cancer high 'tumor monocyte content' was recently found to be a strong predictor for response to immunotherapy and long survival, outperforming tumor lymphocyte content.[330]

In conclusion, a dense myeloid and/or lymphoid infiltrate predicts excellent survival in VSCC patients. A hot tumor immune microenvironment generally is associated with better clinical outcome and improved response to different forms of immunotherapy.[4 30 31] Although many patients with late stage VSCC displayed infiltration by multiple immune cell types, overall this group of patients showed less infiltrating myeloid cells and lymphocytes[7 9] than patients with early stage VSCC. For the clinical application of immunotherapy, this suggests that treatment should be provided as early as possible. Based on these findings a clinical trial exploring the potential of neoadjuvant checkpoint blockade in primary VSCC has started this year (NCT05761132).

Supplemental Figures

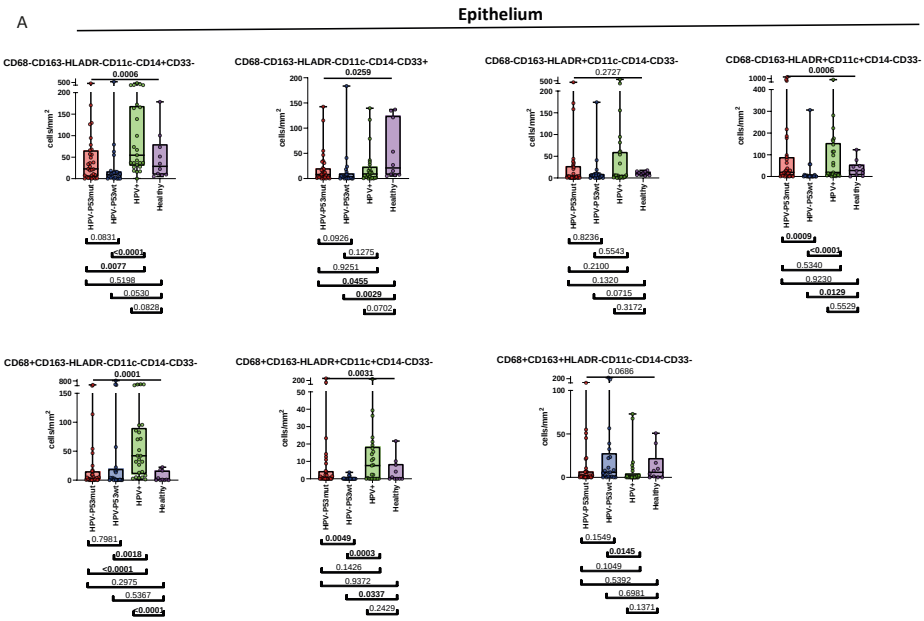

Supplemental Figure 1. Myeloid infiltrate per VSCC molecular subgroup and in healthy vulva.

***A**) Myeloid infiltrate in the epithelium. HPV-P53mut VSCC n=31, HPV-P53wt VSCC n=21, HPV+ VSCC n=25, healthy HPV- vulva n=10. Boxplots with middle line indicating median, colored box indicating interquartile range, vertical lines from minimum to maximum. Kruskal Wallis test derived p-value depicted on top of the boxplots, indicating a significant difference across the four groups. Mann-Whitney U test derived p-values depicted below the boxplots, indicating a significant difference between two groups.*

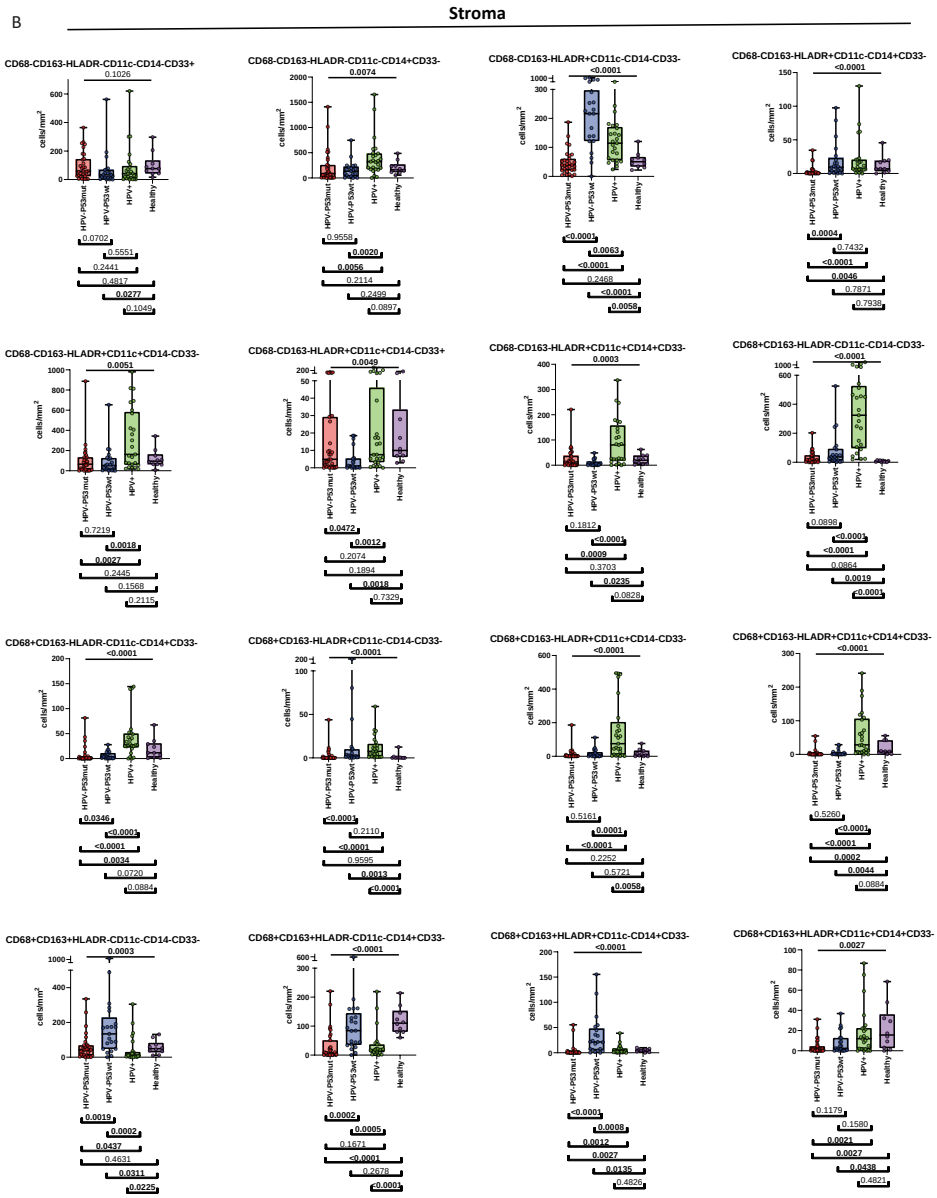

Supplemental Figure 1. Myeloid infiltrate per VSCC molecular subgroup and in healthy vulva.

***B**) Myeloid infiltrate in the stroma. HPV-P53mut VSCC n=31, HPV-P53wt VSCC n=21, HPV+ VSCC n=25, healthy HPV- vulva n=10. Boxplots with middle line indicating median, colored box indicating interquartile range, vertical lines from minimum to maximum. Kruskal Wallis test derived p-value depicted on top of the boxplots, indicating a significant difference across the four groups. Mann-Whitney U test derived p-values depicted below the boxplots, indicating a significant difference between two groups.*

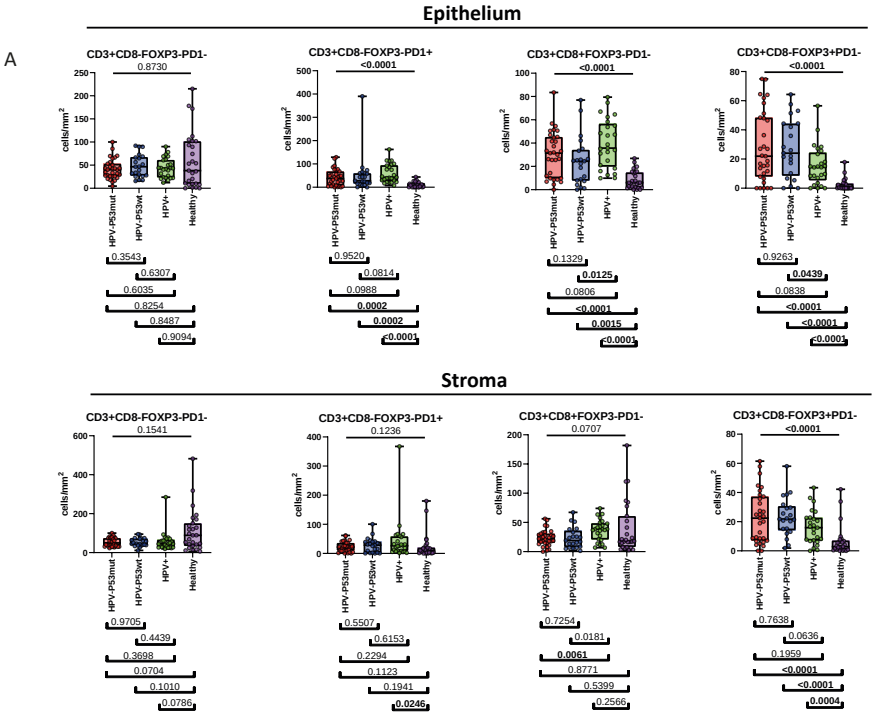

Supplemental Figure 2. Lymphoid infiltrate per VSCC molecular subgroup and in healthy vulva.

***A**) Lymphoid infiltrate in the epithelium. **B**) lymphoid infiltrate in the stroma. HPV-P53mut VSCC n=31, HPV-P53wt VSCC n=21, HPV+ VSCC n=25, healthy HPV- vulva n=27. Boxplots with middle line indicating median, colored box indicating interquartile range, vertical lines from minimum to maximum. Kruskal Wallis test dervied p-value depictend on top of the boxplots, indicating a significant dfiference across the four groups. Mann-Whitney U test derived p-values depicted below the boxplots, indicating a significant difference between two groups.*

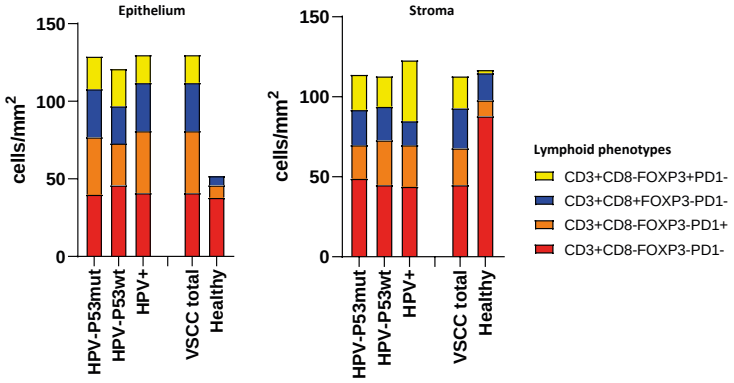

Supplemental Figure 3. No lymphoid immune composition differences across VSCC molecular subgroups.

HPV-P53mut VSCC n=31, HPV-P53wt VSCC n=21, HPV+ VSCC n=25, healthy HPV- vulva n=10.

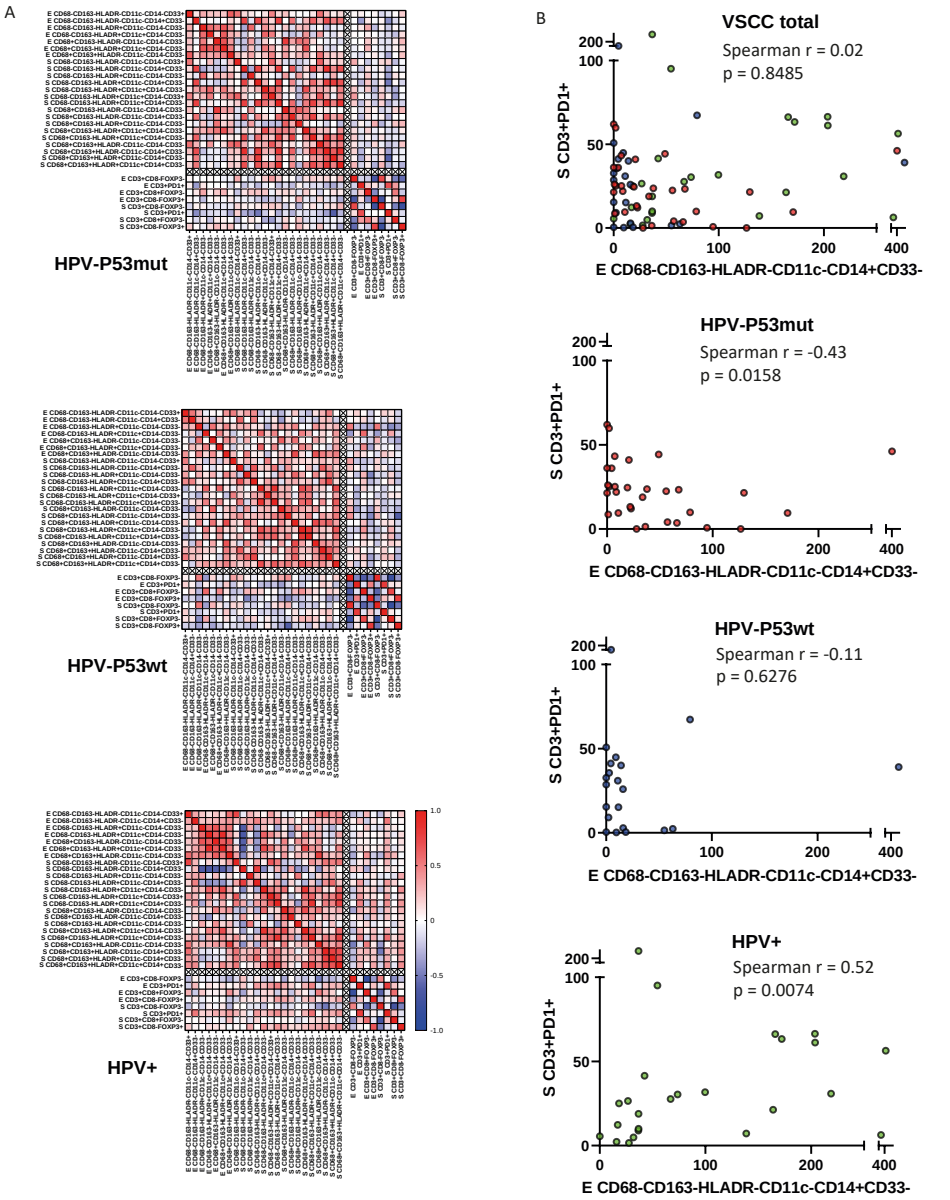

Supplemental Figure 4. Correlation of myeloid and lymphoid immune infiltrate per VSCC molecular subgroup.

A*) Spearman correlation heatmap between myeloid and lymphoid immune phenotypes, per VSCC molecular subgroup. HPV-P53mut VSCC n=31, HPV-P53wt VSCC n=21, HPV+ VSCC n=25.* ***B****) Correlation dot plots between stromal CD3+PD1+ T cells and epithelial CD68-HLADR-CD11c-CD14+CD33- monocytes. Visualized for the total VSCC cohort n=77, and per molecular subgroup separately: HPV-P53mut VSCC (red) n=31, HPV-P53wt VSCC (blue) n=21, HPV+ VSCC (green) n=25.*

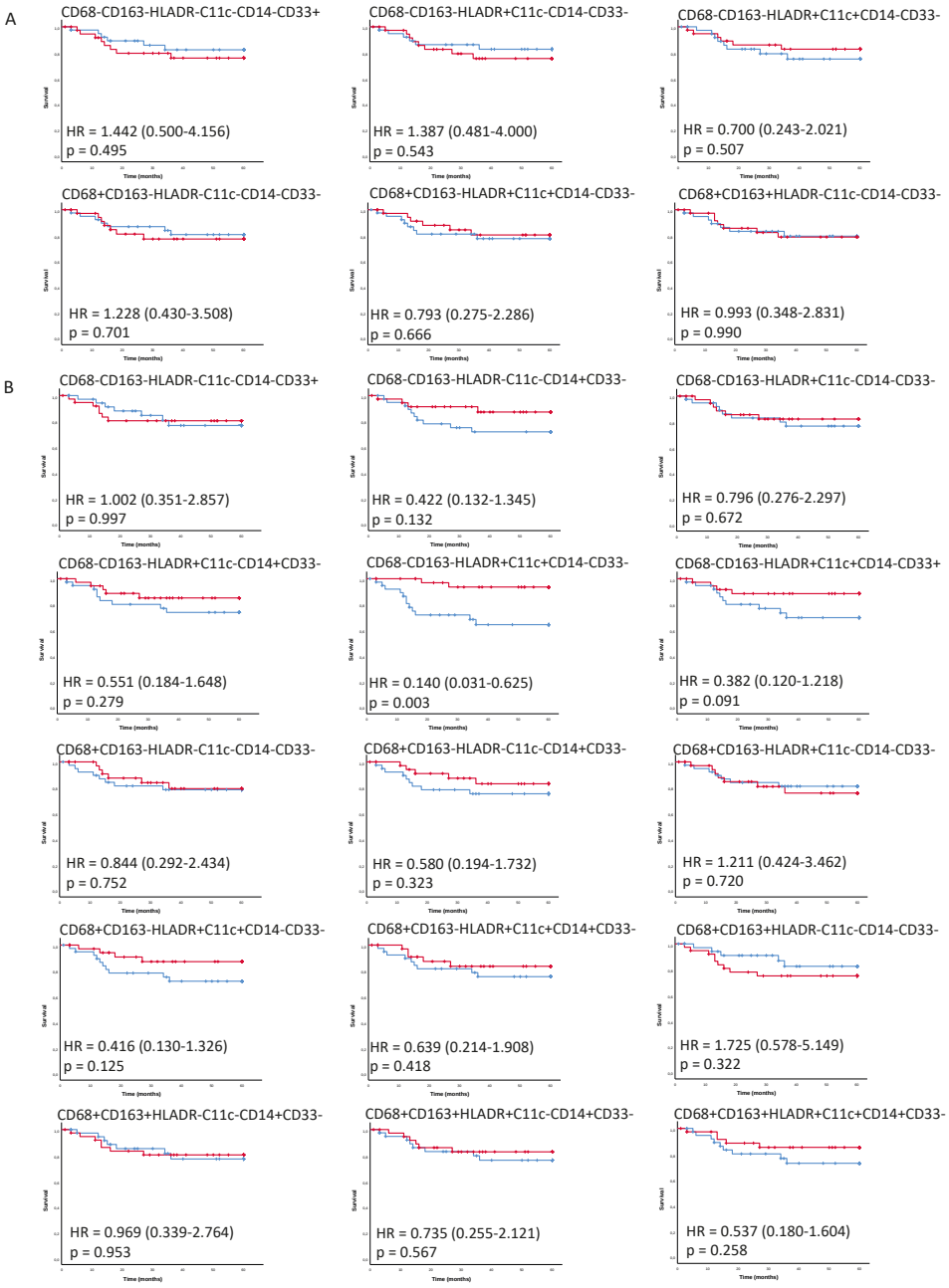

Supplemental Figure 5. Impact of myeloid cell phenotypes presence on survival of VSCC patients.

*The median counts of each myeloid cell phenotype were used to split the total VSCC cohort (n=77) into high (red) or low (blue) infiltrated. The respective Kaplan Meier curves are depicted in **A**) for the epithelial phenotypes and in **B**) for the stromal phenotypes, including the hazard ratio (HR, between brackets the 95% confidence interval of the hazard ratio is provided) and p-value.*

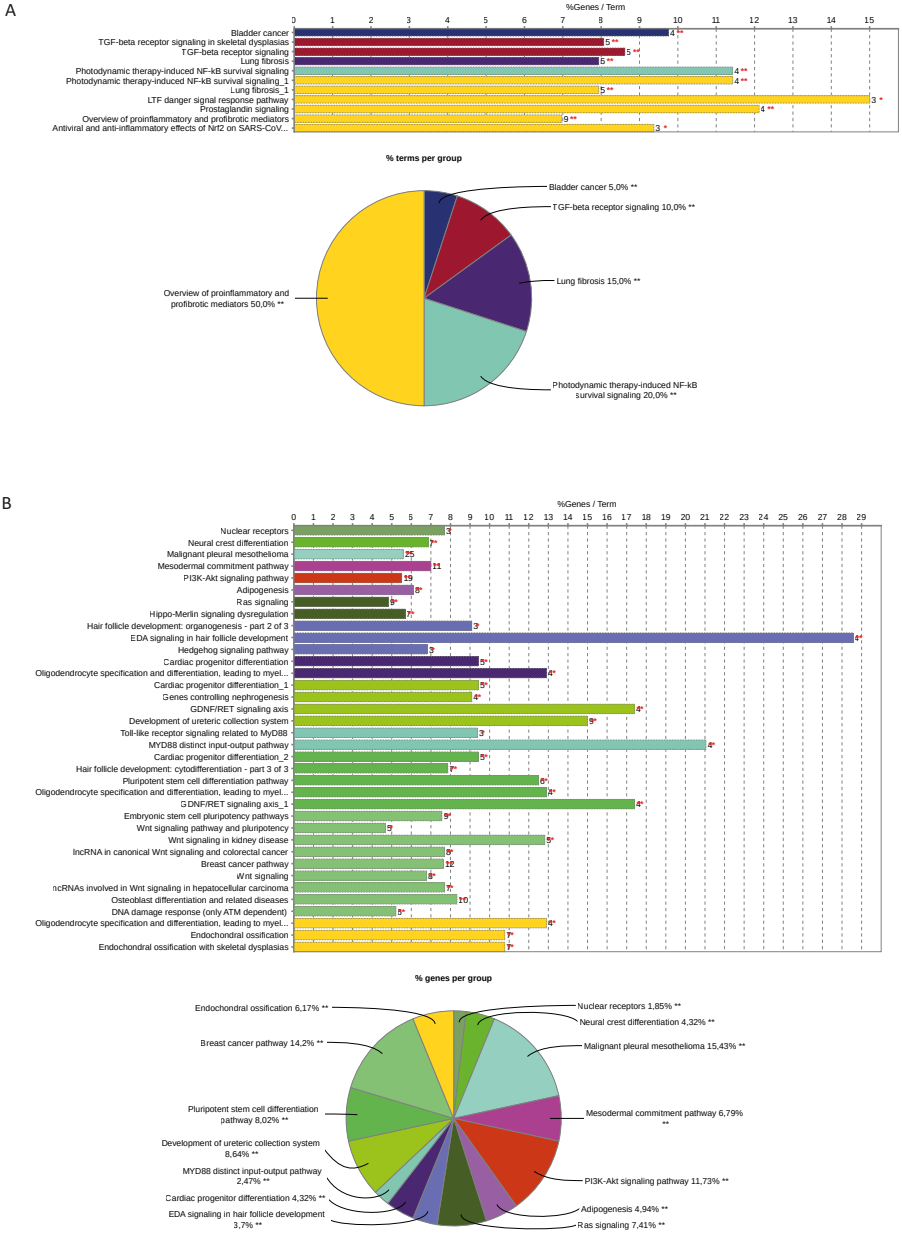

Supplemental Figure 6. Upregulated signaling pathways in monocyte hot and cold VSCC.

***A**) Epithelium monocyte hot (n=39) and in **B**) Epithelium monocyte cold (n=38) VSCC.*

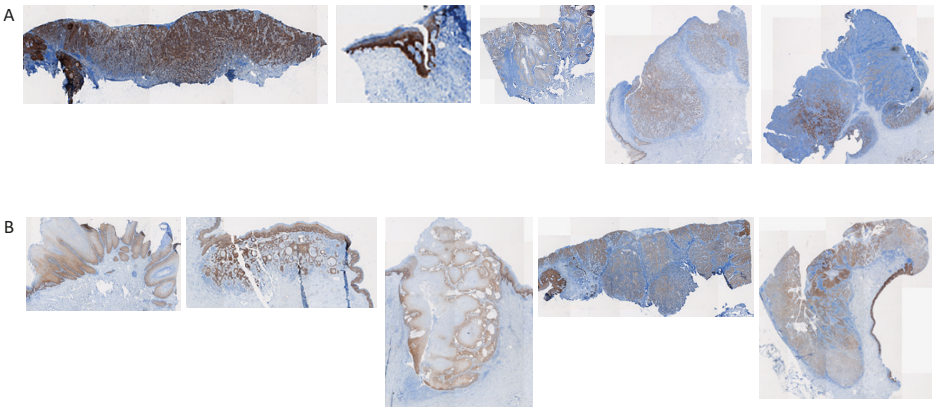

Supplemental Figure 8. Beta-catenin immunohistochemistry on myeloid hot versus cold VSCC.

*10 representative cases of beta-catenin immunohistochemistry in **A**) epithelium myeloid hot (n=5) and **B**) epithelium myeloid cold (n=5) VSCC.*

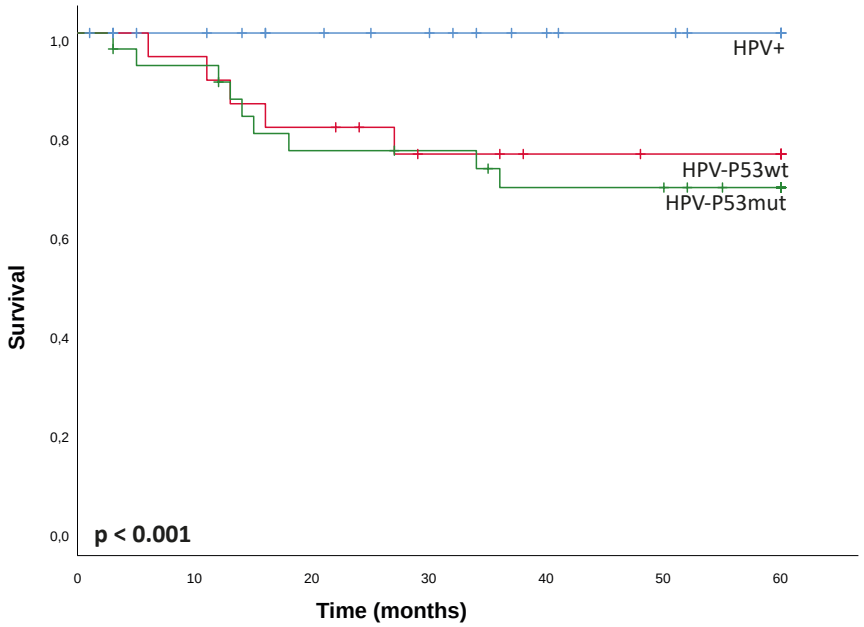

Supplemental Figure 7. Kaplan Meier survival curvers for VSCC, split per molecular subgroup.

VSCC total n=77. HPV-P53mut n=31, HPV-P53wt n=21, HPV+ n=25.

Supplemental Tables

Supplemental Table 1. Patient characteristics

	Healthy HPV- vulva	Early stage (FIGO I/II)	Late stage (FIGO III)
Patients (n)	27	65	12
Age (average, min-max)	-	67 (40-87)	73 (56-93)
Molecular subgroups	-		
HPV-p53mut		22	9
HPV-p53wt		20	1
HPV+		23	2
Therapy (n)	-		
Surgery		64	6
Surgery+radiotherapy		1	6

Supplemental Table 2. VSCC cohort analysed by multispectral immunofluorescence myeloid cell analysis and Nanostring transcriptomic analysis.

	Vectra myeloid panel (104)	Nanostring IO360 (44)	Nanostring PanCancer (34)
HPV-p53mut VSCC	31	17	10
HPV-p53wt VSCC	21	10	9
HPV+ VSCC	25	11	9
Healthy HPV- vulva	27	6	6

Supplemental Table 3. Multispectral immunofluorescence myeloid cell panel design.

Marker	Primary antibody clone and producer	Species and isotype	Dilution	Detection method
HLA-DR	TAL1B5 - Abcam	mouse IgG1	1_50	Directly labelled with Alexa 488
CD11c	EP1347Y - Abcam	rabbit IgG	1_100	Directly labelled with Alexa 546
CD68	D4B9C XP - CST	rabbit IgG	1_50	Directly labelled with Alexa 594
CD14	D7A2T - CST	rabbit IgG	1_25	Indirect with CF Donkey-a-Rabbit IgG 633
CD33	PWS44 - Novocastra	mouse IgG2b	1_25	Indirect with Alexa Goat-a-Mouse IgG2b 647
CD163	10D6 - Invitrogen	mouse IgG1	1_10	Indirect with CF Goat-a-Mouse IgG1 680
DAPI	-	-	1_500	Fluorescent probe

Supplemental Table 4. Myeloid cell phenotype counts in VSCC per stage

	VSCC total			Early stage VSCC			Late stage VSCC			p-value		
Full phenotype	Median	Min	Max	Median	Min	Max	Median	Min	Max	Early vs late stage VSCC	Short phenotype	Cell type name
Epithelium CD68-CD163-HLADR-CD11c-CD14-CD33+	6.16	0.00	183.61	6.05	0.00	183.61	12.44	0.00	116.69	0.4335	Epithelium CD33+rest-	Immature myeloid cell
Epithelium CD68-CD163-HLADR-CD11c-CD14+CD33-	27.66	0.00	587.97	32.00	0.00	587.97	14.00	0.00	401.28	0.058	Epithelium CD14+rest-	Monocyte
Epithelium CD68-CD163-HLADR+CD11c-CD14-CD33-	4.66	0.00	659.03	4.76	0.00	659.03	2.68	0.00	205.80	0.6117	Epithelium HLADR+rest-	HLADR+ cell
Epithelium CD68-CD163-HLADR+CD11c+CD14-CD33-	10.56	0.00	1289.44	9.87	0.00	1289.44	22.68	0.31	217.46	0.2845	Epithelium HLADR+CD11c+rest-	Dendritic cell
Epithelium CD68+CD163-HLADR-CD11c-CD14-CD33-	7.83	0.00	846.63	7.83	0.00	846.63	6.88	0.00	152.25	0.9529	Epithelium CD68+rest-	Macrophage
Epithelium CD68+CD163-HLADR+CD11c+CD14-CD33-	0.00	0.00	285.62	0.00	0.00	285.62	1.39	0.00	12.62	0.6519	Epithelium CD68+HLADR+CD11c+rest-	M1-like macrophage
Epithelium CD68+CD163+HLADR-CD11c-CD14-CD33-	1.35	0.00	224.67	1.17	0.00	224.67	6.30	0.00	102.55	0.1387	Epithelium CD68+CD163+rest-	M2-like macrophage
Stroma CD68-CD163-HLADR-CD11c-CD14-CD33+	42.30	0.00	620.08	41.72	0.00	620.08	90.18	0.22	300.44	0.1477	Stroma CD33+rest-	Immature myeloid cell
Stroma CD68-CD163-HLADR-CD11c-CD14+CD33-	173.14	0.00	1653.71	190.14	0.00	1653.71	8.46	0.00	1013.98	**0.0212**	Stroma CD14+rest-	Monocyte
Stroma CD68-CD163-HLADR+CD11c-CD14-CD33-	79.59	0.00	1093.08	109.25	1.15	1093.08	45.06	0.00	113.28	**0.0029**	Stroma HLADR+rest-	HLADR+ cell
Stroma CD68-CD163-HLADR+CD11c-CD14+CD33-	5.29	0.00	130.08	6.26	0.00	130.08	0.25	0.00	1.22	**<0.0001**	Stroma HLADR+CD14+rest-	Monocyte

Supplemental Table 4 *Continued*

	VSCC total			Early stage VSCC			Late stage VSCC			p-value		
Full phenotype	**Median**	**Min**	**Max**	**Median**	**Min**	**Max**	**Median**	**Min**	**Max**	**Early vs late stage VSCC**	**Short phenotype**	**Cell type name**
Stroma CD68-CD163-HLADR+ CD11c+CD14-CD33-	75.95	0.00	980.41	104.98	0.00	980.41	14.90	1.22	84.59	**0.0025**	Stroma HLADR+CD11c+rest-	Dendritic cell
Stroma CD68-CD163-HLADR+ CD11c+CD14-CD33+	5.20	0.00	369.37	5.20	0.00	369.37	5.03	0.00	65.71	0.9502	Stroma HLADR+CD11c+CD33+rest-	Immature dendritic cell
Stroma CD68-CD163-HLADR+ CD11c+CD14+CD33-	14.04	0.00	337.17	18.45	0.00	337.17	0.11	0.00	26.44	**0.0003**	Stroma HLADR+CD11c+CD14+rest-	Dendritic cell
Stroma CD68+CD163-HLADR- CD11c-CD14-CD33-	41.92	0.00	1390.00	48.20	0.00	1390.00	30.07	2.70	91.05	0.3061	Stroma CD68+rest-	Macrophage
Stroma CD68+CD163-HLADR- CD11c-CD14+CD33-	3.63	0.00	144.26	5.21	0.00	144.26	0.11	0.00	23.75	**0.0033**	Stroma CD68+CD14+rest-	Inflammatory macrophage
Stroma CD68+CD163-HLADR+ CD11c-CD14-CD33-	1.68	0.00	203.82	1.68	0.00	203.82	1.74	0.00	43.85	0.7848	Stroma CD68+HLADR+rest-	M1-like macrophage
Stroma CD68+CD163-HLADR+ CD11c+CD14-CD33-	8.13	0.00	494.83	13.12	0.00	494.83	1.36	0.00	7.58	**0.0083**	Stroma CD68+HLADR+CD11c+rest-	M1-like macrophage
Stroma CD68+CD163-HLADR+ CD11c+CD14+CD33-	1.89	0.00	241.36	4.63	0.00	241.36	0.00	0.00	1.90	**0.0004**	Stroma CD68+HLADR+CD11c+ CD14+rest-	M1-like macrophage
Stroma CD68+CD163+HLADR- CD11c-CD14-CD33-	42.57	0.00	1171.33	37.38	0.00	1171.33	46.35	0.00	257.84	0.7423	Stroma CD68+CD163+rest-	M2-like macrophage
Stroma CD68+CD163+HLADR- CD11c-CD14+CD33-	20.49	0.00	580.58	24.49	0.00	580.58	2.55	0.00	174.41	**0.0014**	Stroma CD68+CD163+CD14+rest-	M2-like macrophage
Stroma CD68+CD163+HLADR+ CD11c-CD14+CD33-	2.09	0.00	155.49	3.13	0.00	155.49	0.14	0.00	1.22	**<0.0001**	Stroma CD68+CD163+HLADR+ CD14+rest-	M2-like macrophage
Stroma CD68+CD163+HLADR+ CD11c+CD14+CD33-	2.28	0.00	86.67	4.57	0.00	86.67	0.00	0.00	10.29	**0.0001**	Stroma CD68+CD163+HLADR+ CD11c+CD14+CD33-	M2-like macrophage

Supplemental Table 5. Lymphoid and myeloid cell counts per VSCC molecular subgroup

A. Myeloid cell counts

	HPV-p53mut VSCC			HPV-p53wt VSCC			HPV+ VSCC			Healthy vulva			p-value							
	Median	Min	Max	Median	Min	Max	Median	Min	Max	Median	Min	Max	HPV-p53mut vs HPV-p53wt VSCC	HPV-p53mut vs HPV+ VSCC	HPV-p53wt vs HPV+ VSCC	HPV-p53mut VSCC vs healthy vulva	HPV-p53wt VSCC vs healthy vulva	HPV+ VSCC vs healthy vulva	Short phenotype	Cell type name
Epithelium CD68-CD163-HLADR-CD11c-CD14-CD33+	8.08	0.00	142.63	3.55	0.00	183.61	9.02	0.00	139.52	21.01	4.97	136.88	0.0926	0.9251	0.1275	**0.0455**	**0.0029**	0.0702	Epithelium CD33+rest-	Immature myeloid cell
Epithelium CD68-CD163-HLADR-CD11c-CD14+CD33-	22.67	0.00	401.28	9.59	0.00	587.97	54.61	0.00	428.19	28.70	4.97	178.72	0.0831	**0.0077**	**<0.0001**	0.5198	0.053	0.0828	Epithelium CD14+rest-	Monocyte
Epithelium CD68-CD163-HLADR+CD11c-CD14-CD33-	3.30	0.00	339.91	6.16	0.00	174.26	5.78	0.00	659.03	10.09	4.78	17.71	0.8236	0.21	0.5543	0.132	0.0715	0.3172	Epithelium HLADR+rest-	HLADR+ cell
Epithelium CD68-CD163-HLADR+CD11c+CD14-CD33-	19.32	0.00	1289.44	0.74	0.00	306.06	18.72	0.98	815.47	27.76	0.00	123.28	**0.0009**	0.534	**<0.0001**	0.923	**0.0129**	0.5529	Epithelium HLADR+CD11c+ rest-	Dendritic cell
Epithelium CD68+CD163-HLADR-CD11c-CD14-CD33-	2.75	0.00	267.33	2.60	0.00	846.63	42.11	1.20	343.11	0.97	0.00	22.46	0.7981	**<0.0001**	**0.0018**	0.2975	0.5367	**<0.0001**	Epithelium CD68+rest-	Macrophage
Epithelium CD68+CD163-HLADR+CD11c+CD14-CD33-	0.57	0.00	285.62	0.00	0.00	3.69	7.63	0.00	260.93	0.48	0.00	21.71	0.0049	0.1426	**0.0003**	0.9372	**0.0337**	0.2429	Epithelium CD68+HLADR+ CD11c+rest-	M1-like macrophage
Epithelium CD68+CD163+HLADR-CD11c-CD14-CD33-	2.00	0.00	102.55	5.88	0.00	224.67	0.00	0.00	73.01	5.85	0.00	50.77	0.1549	0.1049	**0.0145**	0.5392	0.6981	0.1371	Epithelium CD68+CD163+ rest-	M2-like macrophage
Stroma CD68-CD163-HLADR-CD11c-CD14-CD33+	58.43	3.46	364.29	32.68	0.00	562.04	41.72	0.22	620.08	76.65	16.73	297.47	0.0702	0.2441	0.5551	0.4817	**0.0277**	0.1049	Stroma CD33+ rest-	Immature myeloid cell
Stroma CD68-CD163-HLADR-CD11c-CD14+CD33-	87.47	0.00	1411.62	133.82	1.03	747.34	324.88	0.00	1653.71	164.19	56.46	488.17	0.9558	**0.0056**	**0.002**	0.2114	0.2499	0.0897	Stroma CD14+ rest-	Monocyte
Stroma CD68-CD163-HLADR+CD11c-CD14-CD33-	39.13	1.15	186.94	216.50	0.00	1093.08	114.71	24.29	303.58	50.65	21.88	120.50	**<0.0001**	**<0.0001**	**0.0063**	0.2468	**<0.0001**	**0.0058**	Stroma HLADR+ rest-	HLADR+ cell
Stroma CD68-CD163-HLADR+CD11c-CD14+CD33-	0.88	0.00	34.54	9.25	0.00	97.51	7.01	0.00	130.08	6.95	0.00	45.71	**0.0004**	**<0.0001**	0.7432	**0.0046**	0.7871	0.7938	Stroma HLADR+ CD14+rest-	Monocyte
Stroma CD68-CD163-HLADR+CD11c+CD14-CD33-	65.52	0.00	886.84	52.47	0.00	653.51	161.71	16.97	980.41	95.69	6.87	343.71	0.7219	**0.0027**	**0.0018**	0.2445	0.1568	0.2115	Stroma HLADR+ CD11c+rest-	Dendritic cell
Stroma CD68-CD163-HLADR+CD11c+CD14-CD33+	4.90	0.00	121.74	0.97	0.00	18.47	7.56	0.00	369.37	9.99	2.86	151.17	**0.0472**	0.2074	**0.0012**	0.1894	**0.0018**	0.7329	Stroma HLADR+ CD11c+CD33+rest-	Immature dendritic cell

Supplemental Table 5 *Continued*

	HPV-p53mut VSCC			HPV-p53wt VSCC			HPV+ VSCC			Healthy vulva			p-value							
	Median	Min	Max	Median	Min	Max	Median	Min	Max	Median	Min	Max	HPV-p53mut vs HPV-p53wt VSCC	HPV-p53mut vs HPV+ VSCC	HPV-p53wt vs HPV+ VSCC	HPV-p53mut VSCC vs healthy vulva	HPV-p53wt VSCC vs healthy vulva	HPV+ VSCC vs healthy vulva	Short phenotype	Cell type name
Stroma CD68-CD163-HLADR+CD11c+CD14+CD33-	12.71	0.00	220.92	6.01	0.00	48.92	80.52	0.00	337.17	19.80	2.29	62.45	0.1812	**0.0009**	**<0.0001**	0.3703	**0.0235**	0.0828	Stroma HLADR+CD11c+CD14+rest-	Dendritic cell
Stroma CD68+CD163-HLADR-CD11c-CD14-CD33-	15.75	0.00	202.44	37.07	0.58	525.34	324.09	19.34	1390.00	6.91	0.94	14.63	0.0898	**<0.0001**	**<0.0001**	0.0864	**0.0019**	**<0.0001**	Stroma CD68+rest-	Macrophage
Stroma CD68+CD163-HLADR-CD11c-CD14+CD33-	0.95	0.00	81.40	3.16	0.00	27.95	27.23	0.00	144.26	11.50	0.94	67.41	0.0346	**<0.0001**	**<0.0001**	**0.0034**	0.072	0.0884	Stroma CD68+CD14+rest-	Inflammatory macrophage
Stroma CD68+CD163-HLADR+CD11c-CD14-CD33-	0.00	0.00	43.85	2.83	0.00	203.82	7.56	0.53	59.07	0.00	0.00	12.53	<0.0001	**<0.0001**	0.211	0.9595	**0.0013**	**<0.0001**	Stroma CD68+HLADR+rest-	M1-like macrophage
Stroma CD68+CD163-HLADR+CD11c+CD14-CD33-	1.45	0.00	186.19	8.13	0.00	111.53	75.36	1.56	494.83	9.69	0.00	76.44	0.5161	**<0.0001**	**0.0001**	0.2252	0.5721	**0.0058**	Stroma CD68+HLADR+CD11c+rest-	M1-like macrophage
Stroma CD68+CD163-HLADR+CD11c+CD14+CD33-	0.52	0.00	54.82	0.63	0.00	28.82	28.47	0.00	241.36	8.65	0.94	55.59	0.526	**<0.0001**	**<0.0001**	**0.0002**	**0.0044**	0.0884	Stroma CD68+HLADR+CD11c+CD14+rest-	M1-like macrophage
Stroma CD68+CD163+HLADR-CD11c-CD14-CD33-	42.79	0.00	334.89	133.82	0.00	1171.33	10.99	0.00	304.46	49.12	10.14	131.26	0.0019	**0.0437**	**0.0002**	0.4631	**0.0311**	**0.0225**	Stroma CD68+CD163+rest-	M2-like macrophage
Stroma CD68+CD163+HLADR-CD11c-CD14+CD33-	7.66	0.00	220.38	84.43	0.00	580.58	18.68	0.00	218.98	110.33	60.55	213.94	0.0002	0.1671	**0.0005**	**<0.0001**	0.2678	**<0.0001**	Stroma CD68+CD163+CD14+rest-	M2-like macrophage
Stroma CD68+CD163+HLADR+CD11c-CD14+CD33-	0.52	0.00	55.37	21.36	0.00	155.49	2.18	0.00	38.67	5.41	0.00	10.09	<0.0001	**0.0012**	**0.0008**	**0.0027**	**0.0135**	0.4826	Stroma CD68+CD163+HLADR+CD14+rest-	M2-like macrophage
Stroma CD68+CD163+HLADR+CD11c+CD14+CD33-	0.96	0.00	31.21	2.47	0.00	36.90	11.94	0.00	86.67	15.66	0.00	68.54	0.1179	**0.0021**	0.158	**0.0027**	**0.0438**	0.4821	Stroma CD68+CD163+HLADR+0CD11c+CD14+CD33-	M2-like macrophage

B. Lymphoid cell counts

	HPV-p53mut VSCC			HPV-p53wt VSCC			HPV+ VSCC			Healthy vulva			p-value					
	Median	Min	Max	Median	Min	Max	Median	Min	Max	Median	Min	Max	HPV-p53mut vs HPV-p53wt VSCC	HPV-p53mut vs HPV+ VSCC	HPV-p53wt vs HPV+ VSCC	HPV-p53mut VSCC vs healthy vulva	HPV-p53wt VSCC vs healthy vulva	HPV+ VSCC vs healthy vulva
Epithelium CD3+CD8-FOXP3-	40.07	4.64	92.02	40.38	18.29	100	43.13	12.27	90.12	38.27	0	215.12	0.3543	0.6035	0.6307	0.8254	0.8487	0.9094
Epithelium CD3+PD1+	43.45	0	390.36	32.05	0	122.92	42.84	7.29	162.33	8.09	0	43.85	0.0926	0.9251	0.1275	**0.0455**	**0.0029**	0.0702
Epithelium CD3+CD8+FOXP3-	22.02	0	74.66	22.32	0	74.99	35.71	9.88	79.45	6	0	26.86	0.8236	0.21	0.5543	0.132	0.0715	0.3172
Epithelium CD3+CD8-FOXP3+	25.18	0	83.48	30.14	0	54.64	14.37	0	56.5	0.43	0	17.9	**0.0009**	0.534	**<0.0001**	0.923	**0.0129**	0.5529
Stroma CD3+CD8-FOXP3-	49.66	11.05	94.95	40.67	27.35	100	44.89	19.16	284.75	88.97	6.46	482.3	0.9705	0.3698	0.4439	0.0704	0.101	0.0786
Stroma CD3+PD1+	21.47	0	100.59	24.62	0	61.95	26.53	1.61	367.48	10.66	0	180.15	0.5507	0.2294	0.6153	0.1123	0.1941	**0.0246**
Stroma CD3+CD8+FOXP3-	21.78	1.93	58.02	24.85	0	61.5	38.51	6.82	74.1	17.91	2.58	181.7	0.7254	**0.0061**	**0.0181**	0.8771	0.5399	0.2566
Stroma CD3+CD8-FOXP3+	23.55	1.37	67.17	18.71	0	54.13	15.88	0	43.28	2.91	0	42.2	0.7638	0.1959	0.0636	**<0.0001**	**<0.0001**	**0.0004**

Supplemental Table 6. DEG list epithelium CD14+rest- low versus high

Gene	Full name	Panel	Upregulated in	Fold change	Log fold change	p-value	p-adjusted
WNT16	wingless-type MMTV integration site family, member 16	PanCancer	epithelium_low	5.02158	2.32814	0.002986	0.187512
RXRG	retinoid X receptor, gamma	PanCancer	epithelium_low	4.74662	2.2469	0.000282	0.086675
PRLR	prolactin receptor	IO360	epithelium_low	3.53672	1.82241	0.000808	0.114686
PLA2G2A	phospholipase A2, group IIA (platelets, synovial fluid)	IO360	epithelium_low	3.31905	1.73077	0.007248	0.231926
EYA1	EYA transcriptional coactivator and phosphatase 1	PanCancer	epithelium_low	3.11424	1.63888	0.005493	0.187512
NTRK2	neurotrophic tyrosine kinase, receptor, type 2	PanCancer	epithelium_low	2.977	1.57386	0.003532	0.187512
PNOC	prepronociceptin	IO360	epithelium_low	2.95625	1.56377	0.007053	0.231926
MAGEB2	melanoma antigen family B2	IO360	epithelium_low	2.91578	1.54388	0.001649	0.117099
SFRP4	secreted frizzled-related protein 4	IO360	epithelium_low	2.8868	1.52947	0.021551	0.32077
C7	complement component 7	IO360	epithelium_low	2.86066	1.51635	0.001577	0.117099
CCL19	chemokine (C-C motif) ligand 19	IO360	epithelium_low	2.85765	1.51483	0.00423	0.200228
MYB	v-myb avian myeloblastosis viral oncogene homolog	PanCancer	epithelium_low	2.68555	1.42522	0.035954	0.275286
DKK1	dickkopf WNT signaling pathway inhibitor 1	IO360	epithelium_low	2.68522	1.42504	0.013088	0.309756
TSPAN7	tetraspanin 7	PanCancer	epithelium_low	2.56534	1.35915	0.001339	0.168602
GNG7	guanine nucleotide binding protein (G protein), gamma 7	PanCancer	epithelium_low	2.56506	1.35899	0.001863	0.168602
CACNA2D3	calcium channel, voltage-dependent, alpha 2/delta subunit 3	PanCancer	epithelium_low	2.46077	1.29911	0.030215	0.25632
WNT3	wingless-type MMTV integration site family, member 3	PanCancer	epithelium_low	2.41955	1.27474	0.00909	0.187512
RELN	reelin	IO360	epithelium_low	2.36089	1.23933	0.00655	0.231926
HOXA11	homeobox A11	PanCancer	epithelium_low	2.34891	1.23199	0.001922	0.168602
LIFR	leukemia inhibitory factor receptor alpha	PanCancer	epithelium_low	2.33202	1.22158	0.000196	0.086675
MAPK10	mitogen-activated protein kinase 10	PanCancer	epithelium_low	2.32805	1.21912	0.01757	0.196143
CD70	CD70 molecule	IO360	epithelium_low	2.32487	1.21715	0.008576	0.246126
CX3CR1	chemokine (C-X3-C motif) receptor 1	IO360	epithelium_low	2.27442	1.1855	0.001393	0.117099
FGF13	fibroblast growth factor 13	IO360	epithelium_low	2.26704	1.18081	0.00936	0.246126

Gene	Full name	Panel	Upregulated in	Fold change	Log fold change	p-value	p-adjusted
CD19	CD19 molecule	IO360	epithelium_low	2.2274	1.15536	0.033519	0.397624
CCL14	chemokine (C-C motif) ligand 14	IO360	epithelium_low	2.1925	1.13258	0.006223	0.231926
SOX10	SRY (sex determining region Y)-box 10	IO360	epithelium_low	2.13245	1.09251	0.037547	0.410131
GPC4	glypican 4	IO360	epithelium_low	2.09836	1.06926	0.009957	0.25248
ESR1	estrogen receptor 1	IO360	epithelium_low	2.08012	1.05667	0.049051	0.447525
CLEC4E	C-type lectin domain family 4, member E	IO360	epithelium_low	2.06521	1.04629	0.039517	0.410661
IL34	interleukin 34	IO360	epithelium_low	2.05396	1.03841	0.001227	0.117099
AR	androgen receptor	PanCancer	epithelium_low	2.05294	1.03769	0.022308	0.225853
BMP6	bone morphogenetic protein 6	PanCancer	epithelium_low	2.03489	1.02495	0.008948	0.187512
IGF1	insulin-like growth factor 1 (somatomedin C)	PanCancer	epithelium_low	1.98393	0.988358	0.028215	0.254764
TNFSF8	tumor necrosis factor (ligand) superfamily, member 8	IO360	epithelium_low	1.97829	0.984252	0.004608	0.204497
SPIB	Spi-B transcription factor (Spi-1/PU.1 related)	IO360	epithelium_low	1.96382	0.973666	0.043945	0.426813
RASGRP2	RAS guanyl releasing protein 2 (calcium and DAG-regulated)	PanCancer	epithelium_low	1.94941	0.963035	0.0117	0.195634
KIT	v-kit Hardy-Zuckerman 4 feline sarcoma viral oncogene homolog	IO360	epithelium_low	1.94787	0.9619	0.009347	0.246126
DTX1	deltex 1, E3 ubiquitin ligase	PanCancer	epithelium_low	1.94582	0.960377	0.017233	0.196143
GATA3	GATA binding protein 3	PanCancer	epithelium_low	1.94306	0.958328	0.024358	0.23009
NLRP3	NLR family, pyrin domain containing 3	IO360	epithelium_low	1.94305	0.95832	0.022571	0.326021
PDGFD	platelet derived growth factor D	PanCancer	epithelium_low	1.94122	0.956967	0.012457	0.196126
CD45RA		IO360	epithelium_low	1.93371	0.951371	0.039196	0.410661
LILRA1	leukocyte immunoglobulin-like receptor, subfamily A (with TM domain), member 1	IO360	epithelium_low	1.93152	0.94974	0.000355	0.094293
TLR9	toll-like receptor 9	IO360	epithelium_low	1.9281	0.947177	0.020351	0.32077
GLI1	GLI family zinc finger 1	IO360	epithelium_low	1.91837	0.939879	0.007513	0.231926
WNT2B	wingless-type MMTV integration site family, member 2B	IO360	epithelium_low	1.90456	0.929457	0.035289	0.40411
PGPEP1	pyroglutamyl-peptidase I	IO360	epithelium_low	1.86752	0.90112	0.000398	0.094293
PBX1	pre-B-cell leukemia homeobox 1	PanCancer	epithelium_low	1.86136	0.896356	0.008956	0.187512

Supplemental Table 6 *Continued*

Gene	Full name	Panel	Upregulated in	Fold change	Log fold change	p-value	p-adjusted
CD27	CD27 molecule	IO360	epithelium_low	1.85276	0.889677	0.027904	0.360444
TNFRSF10C	tumor necrosis factor receptor superfamily, member 10c, decoy without an intracellular domain	IO360	epithelium_low	1.81427	0.859392	0.021437	0.32077
BCL2	B-cell CLL/lymphoma 2	IO360	epithelium_low	1.7926	0.84205	0.017753	0.32077
BMP7	bone morphogenetic protein 7	PanCancer	epithelium_low	1.7804	0.832204	0.029409	0.25632
FGFR1	fibroblast growth factor receptor 1	IO360	epithelium_low	1.7776	0.829932	0.001207	0.117099
ITGA8	integrin, alpha 8	PanCancer	epithelium_low	1.7633	0.818275	0.008345	0.187512
HLA-DOB	major histocompatibility complex, class II, DO beta	IO360	epithelium_low	1.76238	0.817529	0.032085	0.392761
DUSP8	dual specificity phosphatase 8	PanCancer	epithelium_low	1.73225	0.792647	0.001471	0.168602
PTCH1	patched 1	PanCancer	epithelium_low	1.71463	0.777899	0.005152	0.187512
PLCE1	phospholipase C, epsilon 1	PanCancer	epithelium_low	1.70623	0.770814	0.014797	0.196143
TWIST1	twist family bHLH transcription factor 1	IO360	epithelium_low	1.69899	0.764677	0.014475	0.32077
IL11RA	interleukin 11 receptor, alpha	IO360	epithelium_low	1.67842	0.747103	9.74E-05	0.069174
CXCR2	chemokine (C-X-C motif) receptor 2	IO360	epithelium_low	1.6553	0.727095	0.043767	0.426813
BMP4	bone morphogenetic protein 4	PanCancer	epithelium_low	1.65359	0.725604	0.015807	0.196143
FZD8	frizzled class receptor 8	IO360	epithelium_low	1.64641	0.719323	0.004969	0.207544
INHBB	inhibin, beta B	PanCancer	epithelium_low	1.62932	0.704271	0.041457	0.291147
ANGPT1	angiopoietin 1	IO360	epithelium_low	1.59881	0.676996	0.021686	0.32077
GMIP	GEM interacting protein	IO360	epithelium_low	1.59689	0.675266	0.003052	0.180592
TNFRSF18	tumor necrosis factor receptor superfamily, member 18	IO360	epithelium_low	1.59218	0.671002	0.043784	0.426813
CACNA2D1	calcium channel, voltage-dependent, alpha 2/delta subunit 1	PanCancer	epithelium_low	1.58235	0.662067	0.043329	0.291147
TLR7	toll-like receptor 7	IO360	epithelium_low	1.55965	0.641225	0.021642	0.32077
SOX17	SRY (sex determining region Y)-box 17	PanCancer	epithelium_low	1.54548	0.628055	0.037764	0.275286
TLR5	toll-like receptor 5	IO360	epithelium_low	1.53542	0.618629	0.00665	0.231926
ITGAM	integrin, alpha M (complement component 3 receptor 3 subunit)	IO360	epithelium_low	1.53516	0.618388	0.028609	0.360444
FCGR2B	Fc fragment of IgG, low affinity IIb, receptor (CD32)	IO360	epithelium_low	1.52322	0.607128	0.041387	0.41978

Gene	Full name	Panel	Upregulated in	Fold change	Log fold change	p-value	p-adjusted
DTX4	deltex 4, E3 ubiquitin ligase	IO360	epithelium_low	1.5161	0.600369	0.002935	0.180592
LTBP1	latent transforming growth factor beta binding protein 1	PanCancer	epithelium_high	-1.5031	-0.587941	0.044903	0.293304
CBLC	Cbl proto-oncogene C, E3 ubiquitin protein ligase	PanCancer	epithelium_high	-1.54841	-0.630788	0.010018	0.187512
THBS1	thrombospondin 1	IO360	epithelium_high	-1.64234	-0.715756	0.027971	0.360444
ITGA3	integrin, alpha 3 (antigen CD49C, alpha 3 subunit of VLA-3 receptor)	PanCancer	epithelium_high	-1.67056	-0.74033	0.010078	0.187512
DLL1	delta-like 1 (Drosophila)	PanCancer	epithelium_high	-1.67788	-0.746641	0.003482	0.187512
HMGA2	high mobility group AT-hook 2	PanCancer	epithelium_high	-1.71497	-0.778185	0.040439	0.288715
HEY1	hes-related family bHLH transcription factor with YRPW motif 1	IO360	epithelium_high	-1.84831	-0.88621	0.019721	0.32077
IL1B	interleukin 1, beta	PanCancer	epithelium_high	-1.88886	-0.917519	0.011787	0.195634
IL1R2	interleukin 1 receptor, type II	IO360	epithelium_high	-1.91402	-0.936605	0.009227	0.246126
CCL20	chemokine (C-C motif) ligand 20	IO360	epithelium_high	-1.93099	-0.94934	0.028937	0.360444
CDKN2A	cyclin-dependent kinase inhibitor 2A	IO360	epithelium_high	-2.00863	-1.00621	0.044485	0.426813
EGFR	epidermal growth factor receptor	IO360	epithelium_high	-2.05695	-1.04051	0.022959	0.326021
LAMA3	laminin, alpha 3	PanCancer	epithelium_high	-2.12408	-1.08684	0.017454	0.196143
CXCL8	chemokine (C-X-C motif) ligand 8	PanCancer	epithelium_high	-2.24165	-1.16456	0.013784	0.196143
ATF3	activating transcription factor 3	IO360	epithelium_high	-2.25702	-1.17442	0.000754	0.114686
IL1A	interleukin 1, alpha	PanCancer	epithelium_high	-2.36712	-1.24313	0.013596	0.196143
SPP1	secreted phosphoprotein 1	PanCancer	epithelium_high	-2.42351	-1.2771	0.036716	0.275286
FST	follistatin	PanCancer	epithelium_high	-2.54741	-1.34903	0.006988	0.187512
PLAT	plasminogen activator, tissue	PanCancer	epithelium_high	-2.79442	-1.48255	0.002283	0.175205
MMP3	matrix metallopeptidase 3	PanCancer	epithelium_high	-2.97995	-1.57529	0.015173	0.196143
IL19	interleukin 19	PanCancer	epithelium_high	-3.05106	-1.60931	0.011831	0.195634
COL11A1	collagen, type XI, alpha 1	PanCancer	epithelium_high	-3.07056	-1.6185	0.006294	0.187512

Supplemental Table 7. DEG list stroma CD11c+CD14+HLADR+ DC low versus high

Gene	Full name	Panel	Upregulated in	Fold change	Log fold change	p-value	p-adjusted
MMP7	matrix metallopeptidase 7	IO360	stroma_low	3.57759	1.83899	0.006168	0.600719
PLA2G2A	phospholipase A2, group IIA (platelets, synovial fluid)	PanCancer	stroma_low	3.34884	1.74366	0.02539	0.358192
WNT16	wingless-type MMTV integration site family, member 16	PanCancer	stroma_low	3.14858	1.6547	0.040496	0.408286
NTRK2	neurotrophic tyrosine kinase, receptor, type 2	PanCancer	stroma_low	2.76701	1.46833	0.00779	0.301901
THBS4	thrombospondin 4	PanCancer	stroma_low	2.60774	1.3828	0.043355	0.415933
CD19	CD19 molecule	IO360	stroma_low	2.51996	1.3334	0.013796	0.600719
MAPK10	mitogen-activated protein kinase 10	PanCancer	stroma_low	2.49267	1.31769	0.011159	0.301901
SPP1	secreted phosphoprotein 1	IO360	stroma_low	2.48485	1.31316	0.032011	0.6933
VTCN1	V-set domain containing T cell activation inhibitor 1	IO360	stroma_low	2.46969	1.30433	0.012562	0.600719
TSPAN7	tetraspanin 7	PanCancer	stroma_low	2.45649	1.2966	0.002776	0.298128
KIAA0125	KIAA0125	IO360	stroma_low	2.22003	1.15058	0.042317	0.710285
PPP2R2B	protein phosphatase 2, regulatory subunit B, beta	PanCancer	stroma_low	2.13149	1.09186	0.037946	0.408286
SPIB	Spi-B transcription factor (Spi-1/PU.1 related)	IO360	stroma_low	2.12818	1.08962	0.023691	0.672819
BMP6	bone morphogenetic protein 6	PanCancer	stroma_low	2.03799	1.02715	0.010117	0.301901
GNG7	guanine nucleotide binding protein (G protein), gamma 7	PanCancer	stroma_low	2.02677	1.01918	0.025321	0.358192
RASGRP2	RAS guanyl releasing protein 2 (calcium and DAG-regulated)	PanCancer	stroma_low	1.92994	0.948555	0.014962	0.316773
HEY1	hes-related family bHLH transcription factor with YRPW motif 1	IO360	stroma_low	1.92359	0.943805	0.012766	0.600719
CD45RA		IO360	stroma_low	1.91453	0.936987	0.042347	0.710285
COL4A4	collagen, type IV, alpha 4	PanCancer	stroma_low	1.89996	0.925967	0.041919	0.408548
CD3E	CD3e molecule, epsilon (CD3-TCR complex)	IO360	stroma_low	1.89295	0.920637	0.020958	0.646967
ITGA8	integrin, alpha 8	PanCancer	stroma_low	1.81354	0.858811	0.00627	0.301901
XCL1/2		IO360	stroma_low	1.80668	0.853343	0.034999	0.6933
CD27	CD27 molecule	IO360	stroma_low	1.79559	0.844459	0.037232	0.702875
CCND1	cyclin D1	PanCancer	stroma_low	1.78016	0.832007	0.048953	0.429809

Gene	Full name	Panel	Upregulated in	Fold change	Log fold change	p-value	p-adjusted
CX3CR1	chemokine (C-X3-C motif) receptor 1	IO360	stroma_low	1.76914	0.823046	0.030131	0.6933
ACVR1C	activin A receptor, type IC	IO360	stroma_low	1.74801	0.80571	0.009069	0.600719
HLA-DOB	major histocompatibility complex, class II, DO beta	IO360	stroma_low	1.72889	0.789844	0.038609	0.702875
CD2	CD2 molecule	IO360	stroma_low	1.69351	0.760015	0.032307	0.6933
GPR160	G protein-coupled receptor 160	IO360	stroma_low	1.683	0.751031	0.007286	0.600719
PLCG2	phospholipase C, gamma 2 (phosphatidylinositol-specific)	PanCancer	stroma_low	1.66029	0.731432	0.021809	0.347309
IL11	interleukin 11	IO360	stroma_low	1.6441	0.717302	0.043017	0.710285
MFNG	MFNG O-fucosylpeptide 3-beta-N-acetylglucosaminyltransferase	PanCancer	stroma_low	1.62676	0.702003	0.010627	0.301901
ANGPT1	angiopoietin 1	PanCancer	stroma_low	1.62663	0.701889	0.026252	0.358192
CSF1R	colony stimulating factor 1 receptor	PanCancer	stroma_low	1.61971	0.695736	0.041228	0.408286
FZD8	frizzled class receptor 8	IO360	stroma_low	1.58569	0.665115	0.009855	0.600719
ATM	ATM serine/threonine kinase	PanCancer	stroma_low	1.58538	0.664832	0.00877	0.301901
FUT8	fucosyltransferase 8 (alpha (1,6) fucosyltransferase)	PanCancer	stroma_low	1.55277	0.634845	0.040619	0.408286
EPHA2	EPH receptor A2	PanCancer	stroma_high	-1.50484	-0.589607	0.028638	0.374125
WEE1	WEE1 G2 checkpoint kinase	PanCancer	stroma_high	-1.53782	-0.620886	0.020026	0.347309
CBLC	Cbl proto-oncogene C, E3 ubiquitin protein ligase	PanCancer	stroma_high	-1.53998	-0.622911	0.013276	0.301901
POLD1	polymerase (DNA directed), delta 1, catalytic subunit	PanCancer	stroma_high	-1.55377	-0.635769	0.000623	0.293842
MGMT	O-6-methylguanine-DNA methyltransferase	PanCancer	stroma_high	-1.57061	-0.651326	0.00468	0.301901
POLE2	polymerase (DNA directed), epsilon 2, accessory subunit	PanCancer	stroma_high	-1.62282	-0.698502	0.007173	0.301901
S100A9	S100 calcium binding protein A9	IO360	stroma_high	-1.67235	-0.741878	0.048933	0.731821
RORC	RAR-related orphan receptor C	IO360	stroma_high	-1.73198	-0.792424	0.027904	0.6933
GNG4	guanine nucleotide binding protein (G protein), gamma 4	IO360	stroma_high	-1.73616	-0.795897	0.031855	0.6933
STMN1	stathmin 1	PanCancer	stroma_high	-1.73656	-0.796236	0.022402	0.347309
CDC25C	cell division cycle 25C	PanCancer	stroma_high	-1.76092	-0.816328	0.00305	0.298128
CCNE2	cyclin E2	PanCancer	stroma_high	-1.85641	-0.892515	0.003884	0.298128
KIT	v-kit Hardy-Zuckerman 4 feline sarcoma viral oncogene homolog	IO360	stroma_high	-1.89242	-0.920229	0.013107	0.600719

Supplemental Table 7 *Continued*

Gene	Full name	Panel	Upregulated in	Fold change	Log fold change	p-value	p-adjusted
E2F1	E2F transcription factor 1	PanCancer	stroma_high	-1.912	-0.935084	0.002847	0.298128
CDKN1C	cyclin-dependent kinase inhibitor 1C (p57, Kip2)	IO360	stroma_high	-1.95001	-0.963484	0.003156	0.600719
CDKN2A	cyclin-dependent kinase inhibitor 2A	IO360	stroma_high	-1.9848	-0.988995	0.048343	0.731821
CD70	CD70 molecule	IO360	stroma_high	-1.98893	-0.991991	0.033433	0.6933
PLAT	plasminogen activator, tissue	PanCancer	stroma_high	-2.40789	-1.26777	0.011893	0.301901
EGFR	epidermal growth factor receptor	IO360	stroma_high	-2.41922	-1.27454	0.004965	0.600719
GPC4	glypican 4	PanCancer	stroma_high	-2.47737	-1.30881	0.021889	0.347309
IL23A	interleukin 23, alpha subunit p19	PanCancer	stroma_high	-2.6175	-1.38819	0.008496	0.301901
IL19	interleukin 19	PanCancer	stroma_high	-2.61777	-1.38834	0.035111	0.401402
CNTFR	ciliary neurotrophic factor receptor	PanCancer	stroma_high	-2.73642	-1.45229	0.033622	0.401402
PRLR	prolactin receptor	IO360	stroma_high	-2.76995	-1.46986	0.007426	0.600719
MYB	v-myb avian myeloblastosis viral oncogene homolog	PanCancer	stroma_high	-3.02551	-1.59718	0.02188	0.347309

References

1. Abdulrahman Z, Kortekaas KE, De Vos Van Steenwijk PJ, et al. The immune microenvironment in vulvar (pre) cancer: review of literature and implications for immunotherapy. *Expert Opin Biol Ther* 2018;18(12):1223-33. doi: 10.1080/14712598.2018.1542426 [published Online First: 2018/10/31]
2. Nooij LS, Ter Haar NT, Ruano D, et al. Genomic Characterization of Vulvar (Pre) cancers Identifies Distinct Molecular Subtypes with Prognostic Significance. *Clin Cancer Res* 2017;23(22):6781-89. doi: 10.1158/1078-0432.Ccr-17-1302 [published Online First: 2017/09/14]
3. Camus M, Tosolini M, Mlecnik B, et al. Coordination of intratumoral immune reaction and human colorectal cancer recurrence. *Cancer Res* 2009;69(6):2685-93. doi: 10.1158/0008-5472.Can-08-2654 [published Online First: 2009/03/05]
4. Fridman WH, Galon J, Dieu-Nosjean MC, et al. Immune infiltration in human cancer: prognostic significance and disease control. *Curr Top Microbiol Immunol* 2011;344:1-24. doi: 10.1007/82_2010_46 [published Online First: 2010/06/01]
5. **5.** Abdulrahman Z, de Miranda N, van Esch EMG, et al. Pre-existing inflammatory immune microenvironment predicts the clinical response of vulvar high-grade squamous intraepithelial lesions to therapeutic HPV16 vaccination. *J Immunother Cancer* 2020;8(1) doi: 10.1136/jitc-2020-000563 [published Online First: 2020/03/15]
6. Abdulrahman Z, de Miranda N, Hellebrekers BWJ, et al. A pre-existing coordinated inflammatory microenvironment is associated with complete response of vulvar high-grade squamous intraepithelial lesions to different forms of immunotherapy. *Int J Cancer* 2020;147(10):2914-23. doi: 10.1002/ijc.33168 [published Online First: 2020/06/24]
7. Kortekaas KE, Santegoets SJ, Abdulrahman Z, et al. High numbers of activated helper T cells are associated with better clinical outcome in early stage vulvar cancer, irrespective of HPV or p53 status. *J Immunother Cancer* 2019;7(1):236. doi: 10.1186/s40425-019-0712-z [published Online First: 2019/09/05]
8. Kortekaas KE, Santegoets SJ, Tas L, et al. Primary vulvar squamous cell carcinomas with high T cell infiltration and active immune signaling are potential candidates for neoadjuvant PD-1/PD-L1 immunotherapy. *J Immunother Cancer* 2021;9(10) doi: 10.1136/jitc-2021-003671 [published Online First: 2021/10/31]
9. Kerkelä E, Ala-aho R, Klemi P, et al. Metalloelastase (MMP-12) expression by tumour cells in squamous cell carcinoma of the vulva correlates with invasiveness, while that by macrophages predicts better outcome. *J Pathol* 2002;198(2):258-69. doi: 10.1002/path.1198 [published Online First: 2002/09/19]
10. Brustmann H. Galectin-3 and CD1a-positive dendritic cells are involved in the development of an invasive phenotype in vulvar squamous lesions. *Int J Gynecol Pathol* 2006;25(1):30-7. doi: 10.1097/01.pgp.0000179613.40215.c0 [published Online First: 2005/11/25]
11. Bindea G, Mlecnik B, Hackl H, et al. ClueGO: a Cytoscape plug-in to decipher functionally grouped gene ontology and pathway annotation networks. *Bioinformatics* 2009;25(8):1091-3. doi: 10.1093/bioinformatics/btp101 [published Online First: 2009/02/25]
12. Mootha VK, Lindgren CM, Eriksson KF, et al. PGC-1alpha-responsive genes involved in oxidative phosphorylation are coordinately downregulated in human diabetes. *Nat Genet* 2003;34(3):267-73. doi: 10.1038/ng1180
13. Subramanian A, Tamayo P, Mootha VK, et al. Gene set enrichment analysis: a knowledge-based approach for interpreting genome-wide expression profiles. *Proc Natl Acad Sci U S A* 2005;102(43):15545-50. doi: 10.1073/pnas.0506580102 [published Online First: 20050930]
14. Abdulrahman ea. Tumor specific T cells support chemokine-driven spatial organization of intratumoral immune microaggregates needed for long survival. *journal of ImmunoTherapy of Cancer* 2022
15. Wellenstein MD, Coffelt SB, Duits DEM, et al. Loss of p53 triggers WNT-dependent systemic inflammation to drive breast cancer metastasis. *Nature* 2019;572(7770):538-42. doi: 10.1038/s41586-019-1450-6 [published Online First: 2019/08/02]

16. Bezzi M, Seitzer N, Ishikawa T, et al. Diverse genetic-driven immune landscapes dictate tumor progression through distinct mechanisms. *Nat Med* 2018;24(2):165-75. doi: 10.1038/nm.4463 [published Online First: 2018/01/09]
17. Walton J, Blagih J, Ennis D, et al. CRISPR/Cas9-Mediated Trp53 and Brca2 Knockout to Generate Improved Murine Models of Ovarian High-Grade Serous Carcinoma. *Cancer Res* 2016;76(20):6118-29. doi: 10.1158/0008-5472.Can-16-1272 [published Online First: 2016/08/18]
18. Krawczyk KM, Nilsson H, Allaoui R, et al. Papillary renal cell carcinoma-derived chemerin, IL-8, and CXCL16 promote monocyte recruitment and differentiation into foam-cell macrophages. *Lab Invest* 2017;97(11):1296-305. doi: 10.1038/labinvest.2017.78 [published Online First: 2017/08/02]
19. Le Borgne M, Etchart N, Goubier A, et al. Dendritic cells rapidly recruited into epithelial tissues via CCR6/CCL20 are responsible for CD8+ T cell crosspriming in vivo. *Immunity* 2006;24(2):191-201. doi: 10.1016/j.immuni.2006.01.005 [published Online First: 2006/02/14]
20. Sontheimer C, Liggitt D, Elkon KB. Ultraviolet B Irradiation Causes Stimulator of Interferon Genes-Dependent Production of Protective Type I Interferon in Mouse Skin by Recruited Inflammatory Monocytes. *Arthritis Rheumatol* 2017;69(4):826-36. doi: 10.1002/art.39987 [published Online First: 2016/11/20]
21. Thorsson V, Gibbs DL, Brown SD, et al. The Immune Landscape of Cancer. *Immunity* 2018;48(4):812-30.e14. doi: 10.1016/j.immuni.2018.03.023 [published Online First: 2018/04/10]
22. Mariathasan S, Turley SJ, Nickles D, et al. TGFβ attenuates tumour response to PD-L1 blockade by contributing to exclusion of T cells. *Nature* 2018;554(7693):544-48. doi: 10.1038/nature25501 [published Online First: 2018/02/15]
23. Spranger S, Bao R, Gajewski TF. Melanoma-intrinsic β-catenin signalling prevents anti-tumour immunity. *Nature* 2015;523(7559):231-5. doi: 10.1038/nature14404 [published Online First: 2015/05/15]
24. Yang L, Li A, Lei Q, et al. Tumor-intrinsic signaling pathways: key roles in the regulation of the immunosuppressive tumor microenvironment. *J Hematol Oncol* 2019;12(1):125. doi: 10.1186/s13045-019-0804-8 [published Online First: 2019/11/30]
25. Trujillo JA, Luke JJ, Zha Y, et al. Secondary resistance to immunotherapy associated with β-catenin pathway activation or PTEN loss in metastatic melanoma. *J Immunother Cancer* 2019;7(1):295. doi: 10.1186/s40425-019-0780-0 [published Online First: 2019/11/11]
26. Peng W, Chen JQ, Liu C, et al. Loss of PTEN Promotes Resistance to T Cell-Mediated Immunotherapy. *Cancer Discov* 2016;6(2):202-16. doi: 10.1158/2159-8290.Cd-15-0283 [published Online First: 2015/12/10]
27. Huang MN, Nicholson LT, Batich KA, et al. Antigen-loaded monocyte administration induces potent therapeutic antitumor T cell responses. *J Clin Invest* 2020;130(2):774-88. doi: 10.1172/jci128267 [published Online First: 2019/10/30]
28. Borst J, Ahrends T, Bąbała N, et al. CD4(+) T cell help in cancer immunology and immunotherapy. *Nat Rev Immunol* 2018;18(10):635-47. doi: 10.1038/s41577-018-0044-0 [published Online First: 2018/07/31]
29. Carroll TM, Chadwick JA, Owen RP, et al. Tumor monocyte content predicts immunochemotherapy outcomes in esophageal adenocarcinoma. *Cancer Cell* 2023;41(7):1222-41.e7. doi: 10.1016/j.ccell.2023.06.006 [published Online First: 2023/07/12]
30. Tumeh PC, Harview CL, Yearley JH, et al. PD-1 blockade induces responses by inhibiting adaptive immune resistance. *Nature* 2014;515(7528):568-71. doi: 10.1038/nature13954 [published Online First: 2014/11/28]
31. Amaria RN, Reddy SM, Tawbi HA, et al. Neoadjuvant immune checkpoint blockade in high-risk resectable melanoma. *Nat Med* 2018;24(11):1649-54. doi: 10.1038/s41591-018-0197-1 [published Online First: 2018/10/10]